Molecular Therapy
Nucleic Acids
Original Article

Validation of miR-20a as a Tumor Suppressor Gene in Liver Carcinoma Using Hepatocyte-Specific Hyperactive *piggyBac* Transposons

Jaitip Tipanee,[1,5] Mario Di Matteo,[1,2,5] Warut Tulalamba,[1,5] Ermira Samara-Kuko,[1] Jiri Keirsse,[3,4] Jo A. Van Ginderachter,[3,4] Marinee Khim Chuah,[1,2,6] and Thierry VandenDriessche[1,2,6]

[1]Department of Gene Therapy & Regenerative Medicine, Vrije Universiteit Brussel, 1090 Brussels, Belgium; [2]Center for Molecular & Vascular Biology, Department of Cardiovascular Sciences, University of Leuven, 3000 Leuven, Belgium; [3]Myeloid Cell Immunology Lab, VIB Center for Inflammation Research, Brussels, Belgium; [4]Lab of Cellular and Molecular Immunology, Vrije Universiteit Brussel, Brussels, Belgium

We established a semi-high-throughput *in vivo* screening platform using hyperactive *piggyBac* (hyPB) transposons (designated as *PB-miR*) to identify microRNAs (*miR*s) that inhibit hepatocellular carcinoma (HCC) development *in vivo*, following *miR* overexpression in hepatocytes. *PB-miR*s encoding six different *miR*s from the *miR-17-92* cluster and nine *miR*s from outside this cluster were transfected into mouse livers that were chemically induced to develop HCC. In this slow-onset HCC model, *miR-20a* significantly inhibited HCC. Next, we developed a more aggressive HCC model by overexpression of oncogenic Harvey rat sarcoma viral oncogene homolog ($HRAS^{G12V}$) and *c-MYC* oncogenes that accelerated HCC development after only 6 weeks. The tumor suppressor effect of *miR-20a* could be demonstrated even in this rapid-onset $HRAS^{G12V}$/*c-MYC* HCC model, consistent with significantly prolonged survival and decreased HCC tumor burden. Comprehensive RNA expression profiling of 95 selected genes typically associated with HCC development revealed differentially expressed genes and functional pathways that were associated with *miR-20a*-mediated HCC suppression. To our knowledge, this is the first study establishing a direct causal relationship between *miR-20a* overexpression and liver cancer inhibition *in vivo*. Moreover, these results demonstrate that hepatocyte-specific hyPB transposons are an efficient platform to screen and identify *miR*s that affect overall survival and HCC tumor regression.

INTRODUCTION

MicroRNAs (*miR*s) are small, single-stranded, non-protein-coding RNA molecules that are 22 nt in length, and they have been shown to control cell growth, differentiation, and apoptosis.[1] Consequently, impaired *miR* expression has been implicated in tumorigenesis. Abnormal *miR* expression has been found in both solid and hematopoietic tumors and is associated with altered expression of "classical" oncogenes.[2] Typically, *miR*s located in genomic regions that are amplified in cancer function as oncogenes, whereas *miR*s located in chromosomal regions that are deleted in cancer function as tumor suppressors.[3–6] Notably, expression profiling of both *miR*s and protein-coding genes can be used to improve the accuracy of cancer subtype classification, diagnosis, and prognosis.[7–9] Interestingly, about one-half of the annotated human *miR*s map within fragile regions of chromosomes, which are areas of the genome that are associated with various human cancers.[10] Changes in *miR* expression between normal and tumor cells may not necessarily alter the cancerous phenotype because the main interactions of a given *miR* with its various targets could have antagonistic rather than synergistic or additive biological consequences. In particular, some *miR*s are organized in clusters, and the role of each *miR* within a given cluster would need to be assessed for each *miR* individually. To validate a *miR* for diagnostic and therapeutic purposes, it is therefore essential to first establish a causal relationship between its differential expression and the cancerous phenotype in *in vivo* models.

The present study aims at addressing some of these outstanding questions in *miR* biology and cancer using hepatocellular carcinoma (HCC) as a model, given its poor prognosis and high prevalence. HCC is one of the most common causes of cancer-related mortality worldwide.[11,12] The altered expression of several *miR*s (i.e., *miR-18*, *miR-20a*, *miR-21*, *miR-34*, *miR-17-92*, *let-7a*, *let-7c*, *miR-92*, *miR-122*, *miR-195*, *miR*-199a, *miR-200a*, *miR-341*, and *miR-370*) has been associated with HCC in mice and/or humans, but experimental evidence establishing a causal relationship between abnormal expression of these *miR*s and HCC is generally lacking.[13–26] Nevertheless, using *miR* microarray analysis in paired patient-derived samples of

Received 31 August 2019; accepted 13 January 2020;
https://doi.org/10.1016/j.omtn.2020.01.015.

[5]These authors contributed equally to this work.

[6]Senior author

Correspondence: Thierry VandenDriessche, Department of Gene Therapy & Regenerative Medicine, Vrije Universiteit Brussel, Building D, Room D365, Laarbeeklaan 103, 1090 Brussels, Belgium.
E-mail: thierry.vandendriessche@vub.be
Correspondence: Marinee Khim Chuah, Department of Gene Therapy & Regenerative Medicine, Vrije Universiteit Brussel, Building D, Room D365, Laarbeeklaan 103, 1090 Brussels, Belgium.
E-mail: marinee.chuah@vub.be

tumoral tissue and non-tumoral adjacent tissues, several *miR*s (i.e., *miR-92*, *miR-20*, *miR-18*, and *miR-18* precursor) were found to be inversely correlated with the degree of HCC differentiation.[27] Of particular interest is *miR-20a*, a member of the *miR-17-92* cluster, because it increases cell apoptosis and inhibits cell proliferation and migration in transformed HCC cell lines *in vitro*.[14,15] In addition, downregulation of *miR-20a* was observed in primary HCC of patients following liver transplantation.[14] Hence, this suggests a possible role between *miR-20a* and HCC initiation and/or progression. However, formal proof that overexpression of *miR-20a* results in suppression of HCC in cancer models *in vivo* is lacking.

Consequently, establishing a causal relationship between a given *miR* and malignancy following hepatic overexpression of the *miR* should allow us to strengthen the intrinsic diagnostic and therapeutic relevance of *miR*s in HCC and exclude unrelated associations between *miR* expression levels and the cancerous phenotype. In the current study, we designed a hepatocyte-directed gene expression platform for *in vivo miR* screening and validation based on hyperactive *piggyBac* (hyPB) transposons that stably express *miR* from a robust hepatocyte-specific promoter, thereby avoiding ectopic expression in non-liver tissues.[28–30] Co-delivery of PB transposons and constructs expressing PB transposases results in DNA transposition into the target genome through a cut-and-paste mechanism.[31,32] Consequently, PB transposon-based gene transfer offers the advantage of sustained gene expression following genomic integration.[30–35] We also used this PB platform to develop a rapid-onset model for HCC based on the selective hepatocyte-specific overexpression of oncogenic Harvey rat sarcoma viral oncogene homolog ($HRAS^{G12V}$) and *c-MYC* oncogenes that overcomes some of the limitations of current HCC models such as slow onset of tumor development, non-specific expression or effects unrelated to HCC, and time-consuming generation of transgenic models.[36] Using this hepatocyte-specific PB system to functionally screen *miR-17-92* cluster members *in vivo*, we identified *miR-20a* as a tumor suppressor gene in two complementary HCC models, both the conventional slow-onset chemically induced HCC model and the rapid-onset $HRAS^{G12V}$/*c-MYC* HCC model.

RESULTS

Hepatocyte-Specific hyPB Transposon System for Liver-Targeted Overexpression of Exogenous miRs *In Vivo*

We first established an *in vivo* screening platform based on PB transposons that were designed to specifically express any given *miR* in hepatocytes. *miR*s associated with HCC were specifically selected, based primarily on previous studies in cell lines.[13–15] We focused primarily on the *miR*s from the *miR-17-92* cluster, namely *miR-17*, *miR-18a*, *miR-19a*, *miR-20a*, *miR-19b-1*, and *miR-92a-1*. In addition, other *miR*s that are differentially expressed in HCC (i.e., *miR-370*, *miR-1188*, *miR-341*, *miR-221*, *miR-222*, *miR-106b-25*, *miR-93*, *miR-106b*, and *miR-25*) were also tested since it is unclear whether they have a direct impact on tumor growth in liver cancer. The respective *miR* genes and approximately 50–200 bp of the surrounding genomic sequence were PCR amplified from mouse genomic DNA. Subsequently, because in general *miR*s are frequently located within introns, these *miR*-containing fragments were cloned into an intron present in a human FIX mini-gene (designated as *hFIXIA*). One of the main advantages of this platform is that the *miR* gene is then embedded in the FIX mini-gene, which encodes a secretable FIX protein that serves as reporter. This facilitates the continuous monitoring of *in vivo* expression kinetics and determination of transfection efficiency because FIX was proven to be non-immunogenic after liver-directed gene therapy.[28–30] To ensure hepatocyte-specific *miR* expression, a robust *de novo* designed hepatocyte-specific promoter was used that was composed of the transthyretin (TTR_{min}) minimal promoter linked to a hepatocyte-specific *cis*-regulatory module (designated as *HS-CRM8*), which was identified by genome-wide data mining.[28–30]

The expression cassette containing the *HS-CRM8-*TTR_{min} hepatocyte-specific promoter driving the expression of the *hFIXIA* minigene harboring the *miR* gene was inserted into the PB transposon, which was flanked by its inverted repeats (IRs) (Figure 1). All of the distinct *miR*s (i.e., *miR-17*, *miR-19a*, *miR-18a*, *miR-20a*, *miR-19b-1*, or *miR-92a-1*) are encoded by the same factor IX (FIX) transgene and embedded in exactly the same configuration within the first intron (*intron IA*) of this FIX transgene. Since the design of all the *PB-hFIXIA-miR* transposons is identical for each *miR*, FIX serves as an appropriate surrogate reporter gene whose expression can be readily monitored over time in the plasma of the recipient animals without sacrificing the mice.[37–40] The *miR* gene is ideally positioned within intron A of the *hFIXIA* minigene to directly link its expression driven from the *HS-CRM8-*TTR_{min} hepatocyte-specific promoter to that of the FIX protein as reporter. This intron-based *miR* design was successfully implemented and validated in other studies, albeit with distinct reporter genes.[37–40]

We first performed a proof-of-concept study to validate the hepatocyte-specific hyPB transposon system for *miR* overexpression in normal C57BL/6JRj mice (Figure 2). Normal C57BL/6JRj male mice were subjected to hydrodynamic co-transfection of the *PB-hFIXIA-miR* transposon individually expressing each member of the *miR-17-92* cluster (i.e., *miR-17*, *miR-19a*, *miR-18a*, *miR-20a*, *miR-19b-1*, or *miR-92a-1*) in conjunction with a plasmid encoding a hyperactive PB transposase (hyPBase). Control C57BL/6JRj mice were co-transfected with *PB-hFIXIA* devoid of any *miR* and the hyPBase-encoding plasmid. The hFIX reporter gene was stably expressed at high levels that were not significantly different among each of the different *miR*-containing transposon constructs (Figure 2A). This indicates consistent stable transfection efficiencies and transposition across all cohorts. Stable FIX expression was depending on the expression of hyPBase since expression declined to about ~90% of the initial levels at 10 days post-transfection in the absence of any hyPBase (Figure 2A). This indicates that prolonged expression of the FIX/*miR* constructs was mainly determined by hyPBase-mediated stable transposition.

Mice were subsequently euthanized to assess *miR* expression levels after PB-mediated transposition in the mouse livers. Typically, a significant increase in *miR* expression levels could be attained following

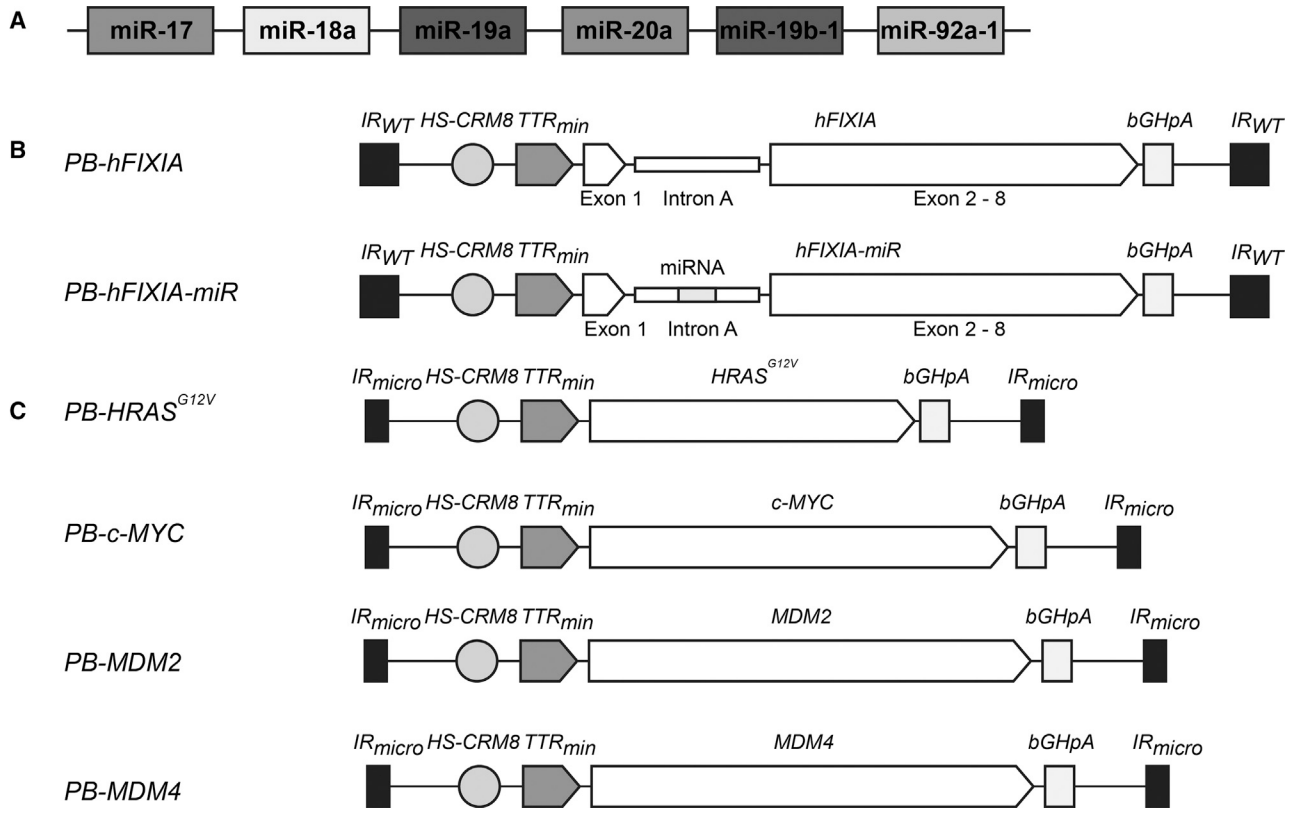

Figure 1. Schematic Representation of Hepatocyte-Specific PB Transposons

(A) Organization of *miR-17-92* cluster members within *PB-hFIXIA-miR-17-92*. (B) *PB-hFIXIA* contains the human factor IX (*hFIX*) gene harboring 1.4 kb of truncated intron A, designated *hFIXIA*, and *PB-hFIXIA-miR* was derived from *PB-hFIXIA* by inserting the corresponding *miR* gene (i.e., *miR-17*, *miR-18a*, *miR-19a*, *miR-20a*, *miR-19b-1*, and *miR-92* a-1) into intron A. Both transposons carry a wild-type inverted repeat (IR_{wt}). (C) *PB-HRAS*^{G12V}, *PB-c-MYC*, *PB-MDM2*, and *PB-MDM4* encode the constitutively active form of Harvey rat sarcoma virus oncogene (HRAS) with a G12V amino acid mutation, the myelocytomatosis oncogene (c-MYC), the transformed mouse 3T3 cell double minute 2 (MDM2) oncogenic protein, and the transformed mouse 3T3 cell double minute 4 (MDM4) oncogenic protein, respectively. All PB transposons expressing oncogenic proteins contain truncated inverted repeats (IR_{micros}). A liver-specific chimeric promoter composed of the minimal transthyretin (TTR_{min}) promoter and hepatocyte-specific *cis*-regulatory module (*HS-CRM8*) was used to drive gene expression in all PB constructs. The bovine growth hormone polyadenylation (bGH-polyA) functioned as a terminating signal.

transfection of mouse livers with *PB-hFIXIA-miR*s and hyPB compared to the controls devoid of *miR* (i.e., *PB-hFIXIA* and hyPB) (Figure 2B). An average 15-fold increase in miR expression was observed after *in vivo* transfection with the *PB-hFIXIA-miR* transposons in normal C57BL/6jRj mice. Comparable levels of hFIX reporter gene expression, relative expression of *hFIX* mRNA, and PB transposon copy number confirmed that the transfection efficiency was similar among *PB-hFIXIA-miRs*/*hyPBase* versus *PB-hFIXIA*/*hyPBase* cohorts (Figures 2A, 2C, and 2D. Collectively, these data validate the hepatocyte-specific hyPB system as a versatile platform to efficiently overexpress selected *miR*s in hepatocytes, making it a suitable system to assess the impact of *miR* overexpression on HCC initiation and/or progression in mice.

Hepatocyte-Specific hyPB Transposon System for the Functional Screening of *miR* in a Slow-Onset HCC Model

Next, the impact of *miR* overexpression on hepatocarcinogenesis was first assessed following PB transposon-mediated hepatic gene delivery in a slow-onset, chemically induced mouse model of HCC. HCC formation was pre-induced by diethylnitrosamine (DEN) in C57BL/6JRj male mice, followed by hydrodynamic transfection of the *PB-hFIXIA-miR*s or *PB-hFIXIA* control using the hyPB system, as previously described.[30] The mice were then euthanized at 36 weeks post-DEN injection to assess tumor burden. Notably, the results showed that *miR-20a* led to a significant reduction in tumor burden based on the reduction in HCC tumor size and number of HCC tumor nodules between mice transfected with the *PB-hFIXIA-miR-20a* transposon and the control *PB-hFIXIA* transposon, which lacked any *miR* ($p < 0.05$) (Figures 3A–3C). Consistently, *miR-20a* expression was selectively and significantly increased up to 28-fold and sustained in the livers of recipient mice that were transfected with the *PB-hFIXIA-miR-20a* transposon and the hyPB transposase (Figure 3D). Significant *miR* overexpression was also observed in the mice transfected with *PB-hFIXIA-miR-17* (~7-fold), *PB-hFIXIA-miR-18a* (~22-fold), *PB-hFIXIA-miR-19a* (~27- fold), *PB-hFIXIA-miR-19b-1* (~14-fold), or *PB-hFIXIA-miR-92a-1* (~19-fold), respectively (Figure 3D). An average 20-fold increase in *miR* expression was observed after *in vivo* transfection with the *PB-hFIXIA-miR*

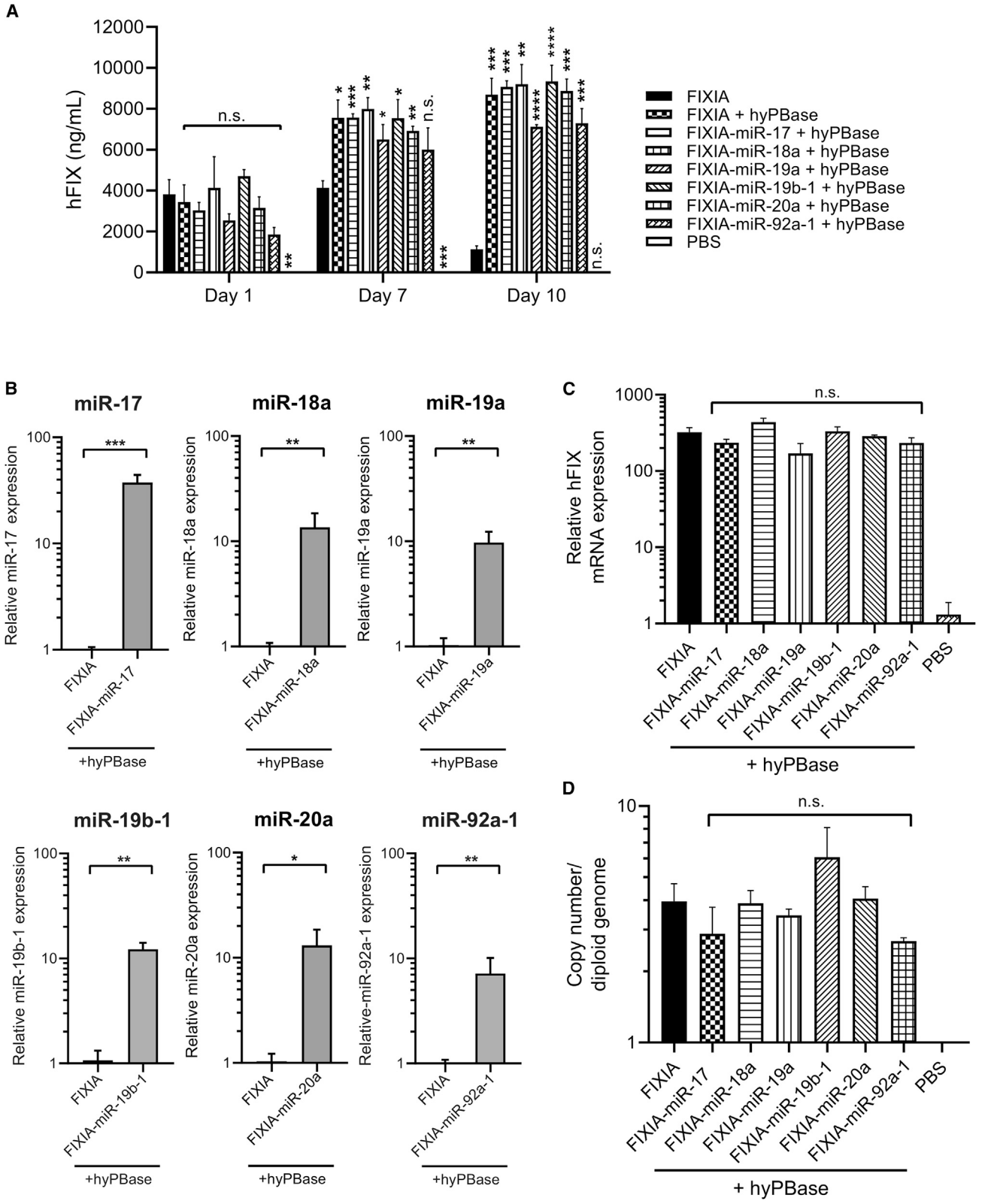

(legend on next page)

transposons in the slow-onset DEN-treated C57BL/6jRj mouse model. However, it did not contribute to a significant difference of HCC tumor sizes and nodule numbers compared to the control *PB-hFIXIA/hyPBase* mice ($p > 0.05$) (Figures 3B and 3C). Similar results were obtained based on *miR*s that did not belong to the *miR-17-92* cluster but that were differentially expressed in HCC, such as *miR-370*, *miR-1188*, *miR-341*, *miR-221*, *miR-222*, *miR-106b-25*, *miR-93*, and *miR-25* (Figure S1). Although a slight reduction in tumor size was apparent in the case of *miR-106b*, the number of tumor nodules was not statistically significantly different from that of controls (Figure S1). The *PB-hFIXIA-miR* transposons were efficiently transfected into the mouse liver of the DEN-treated mice and stably expressed the hFIX protein (Figure 3E) that is encoded by the *miR*-containing FIX transcripts (Figure 1). There are no significant differences in expression among the different *miR*-containing constructs, in accordance with the comparable FIX protein levels obtained with each *PB-hFIXIA-miR* transposon encoding *miR-17*, *miR-19a*, *miR-18a*, *miR-20a*, *miR-19b-1*, or *miR-92a-1* (Figure 3E). This is consistent with the comparable PB transposon copy numbers per diploid genome among the different cohorts (Figure 3F) and with the results obtained in normal C57BL/6JRj mice (Figure 2).

Collectively, these results suggest that *miR-20a* is a tumor suppressor gene that inhibits HCC development and/or progression in the slow-onset DEN-induced murine model. This justifies the focus of the subsequent studies on *miR-20a* since it is only *miR-20a* that has tumor suppressor effects in the slow-onset DEN-induced HCC model.

Establishment and Characterization of the Rapid-Onset HCC Model

One of the limitations of the DEN chemically induced HCC model is the slow onset of HCC development. This reflects, at least in part, the random nature of the DEN-induced mutations. Although transgenic cancer models with a more rapid tumor progression have been developed, the effects are not always cell type-specific since ubiquitous promoters are often employed over cell type-specific ones. Moreover, such transgenic models are based on germline modifications and often lead to developmental perturbations. Typically, germline modifications in transgenic models do not adequately model the effect of somatic oncogene activation in adults. To overcome the limitations of existing HCC models, we first developed an HCC model using the PB transposon platform to simultaneously overexpress somatically multiple oncogenes in hepatocytes of adult mice. Previous studies have shown that dysregulation of the ras viral oncogene homolog (Ras) and c-Myc oncogene-dependent pathways promotes malignant transformation and tumor progression in the liver.[41,42] In addition, transformed mouse 3T3 cell double minute 2 (*MDM2*) and *MDM4* act as oncogenes and induce HCC by targeting the tumor suppressor p53.[43,44] Hence, $HRAS^{G12V}$, *c-MYC*, *MDM2*, and *MDM4* are attractive candidate oncogenes to establish a rapid-onset HCC model by somatic gene transfer in adult hepatocytes.

PB transposons were therefore designed that expressed $HRAS^{G12V}$, *c-MYC*, *MDM2*, or *MDM4* under the control of the hepatocyte-specific TTR_{min}/*HS-CRM8* promoter (Figure 1).[29] Subsequently, *PB-*$HRAS^{G12V}$ was co-transfected in combination with *PB-c-MYC*, *PB-MDM2*, or *PB-MDM4* transposons using the hyPB platform. HCC tumor nodules were present in mouse livers stably transfected with the *PB-*$HRAS^{G12V}$*/PB-c-MYC* combination, whereas the other combinations (i.e., *PB-*$HRAS^{G12V}$*/PB-MDM2* or *PB-*$HRAS^{G12V}$*/PB-MDM4*) and single oncogene expression (i.e., *PB-*$HRAS^{G12V}$ or *PB-c-MYC*) did not induce any liver tumor development (Figures 4A and 4B). This is consistent with a possible cooperativity between the $HRAS^{G12V}$ and *c-MYC* oncogenes allowing rapid-onset HCC development. We observed the pathological abnormalities only in

Figure 2. Validation of Hepatocyte-Specific hyPB Transposon Platform for Overexpression of the *miR-17-92* Cluster Members in Normal Mice

Six-week-old C57BL/6JRj male mice were hydrodynamically transfected with 10 μg of either the *PB-hFIXIA-miR* or *PB-hFIXIA* construct and 2 μg of PB transposase-encoding plasmid. Mice transfected with *PB-hFIXIA* without PB transposase-encoding plasmid and PBS-injected mice were used as a controls (*PB-hFIXIA*, n = 3 mice; *PB-hFIXIA+hyPBase*, n = 3 mice; *PB-hFIXIA-miR-17+hyPBase*, n = 3 mice; *PB-hFIXIA-miR-18a+hyPBase*, n = 3 mice; *PB-hFIXIA-miR-19a+hyPBase*, n = 3 mice; *PB-hFIXIA-miR-19b-1+hyPBase*, n = 3 mice; *PB-hFIXIA-miR-20a+hyPBase*, n = 3 mice; *PB-hFIXIA-miR-92a-1+hyPBase*, n = 3 mice). (A) hFIX protein expression analysis on days 1, 7, and 10 post-transfection measured by enzyme-linked immunosorbent assay (ELISA) to monitor the transfection efficiency of the PB transposons. Graph represents the mean ± SEM of data obtained from individual mice; unpaired Student's t test (n.s., not significant; *$p < 0.05$, **$p < 0.01$, ***$p < 0.001$). *PB-hFIXIA-miR/hyPBase*-treated mice were compared to the *PB-hFIXIA* control group devoid of *hyPBase* (*PB-hFIXIA*, n = 3 mice; *PB-hFIXIA+hyPBase*, n = 3 mice; *PB-hFIXIA-miR-17+hyPBase*, n = 3 mice; *PB-hFIXIA-miR-18a+hyPBase*, n = 3 mice; *PB-hFIXIA-miR-19a+hyPBase*, n = 3 mice; *PB-hFIXIA-miR-19b-1+hyPBase*, n = 3 mice; *PB-hFIXIA-miR-20a+hyPBase*, n = 3 mice; *PB-hFIXIA-miR-92a-1+*hyPBase, n = 3 mice). (B) Quantitative miR expression levels in the mouse liver on day 10 post-transfection measured by quantitative PCR (qPCR) to assess the elevated selected miR expression in *PB-hFIXIA-miRs/hyPBase*-treated mice compared to control devoid of miR (i.e., *PB-hFIXIA/hyPBase*). Graph represents the mean ± SEM of data obtained from individual mice; two-tailed unpaired Student's t test (n.s., not significant; *$p < 0.05$, **$p < 0.01$) (*PB-hFIXIA*, n = 3 mice; *PB-hFIXIA+hyPBase*, n = 3 mice; *PB-hFIXIA-miR-17+hyPBase*, n = 3 mice; *PB-hFIXIA-miR-18a+hyPBase*, n = 3 mice; *PB-hFIXIA-miR-19a+hyPBase*, n = 3 mice; *PB-hFIXIA-miR-19b-1+hyPBase*, n = 3 mice; *PB-hFIXIA-miR-20a+hyPBase*, n = 3 mice; *PB-hFIXIA-miR-92a-1+hyPBase*, n = 3 mice). (C) Relative hFIX mRNA expression levels in mouse livers on day 10 post-transfection measured by qPCR to assess the relative hFIX mRNA expression in the *PB-hFIXIA-miR/hyPBase*-treated mice compared to the *PB-hFIXIA/hyPBase* control group. Graph represents the mean ± SEM of data obtained from individual mice; two-tailed unpaired Student's t test (n.s., not significant; *$p < 0.05$, **$p < 0.01$, ***$p < 0.001$) (*PB-hFIXIA*, n = 3 mice; *PB-hFIXIA+hyPBase*, n = 3 mice; *PB-hFIXIA-miR-17+hyPBase*, n = 3 mice; *PB-hFIXIA-miR-18a+hyPBase*, n = 3 mice; *PB-hFIXIA-miR-19a+hyPBase*, n = 3 mice; *PB-hFIXIA-miR-19b-1+hyPBase*, n = 3 mice; *PB-hFIXIA-miR-20a+hyPBase*, n = 3 mice; *PB-hFIXIA-miR-92a-1+hyPBase*, n = 3 mice). (D) Quantitative PB transposon copy number per diploid genome in the mouse liver on day 10 post-transfection measured by qPCR. All *PB-hFIXIA-miR/hyPBase*-treated groups were statistically compared to *PB-hFIXIA/hyPBase* control group. Graph represents the mean ± SEM of data obtained from individual mice; two-tailed unpaired Student's t test (n.s., not significant; *$p < 0.05$, **$p < 0.01$, ***$p < 0.001$) (*PB-hFIXIA*, n = 3 mice; *PB-hFIXIA+hyPBase*, n = 3 mice; *PB-hFIXIA-miR-17+hyPBase*, n = 3 mice; *PB-hFIXIA-miR-18a+hyPBase*, n = 3 mice; *PB-hFIXIA-miR-19a+hyPBase*, n = 3 mice; *PB-hFIXIA-miR-19b-1+hyPBase*, n = 3 mice; *PB-hFIXIA-miR-20a+hyPBase*, n = 3 mice; *PB-hFIXIA-miR-92a-1+hyPBase*, n = 3 mice).

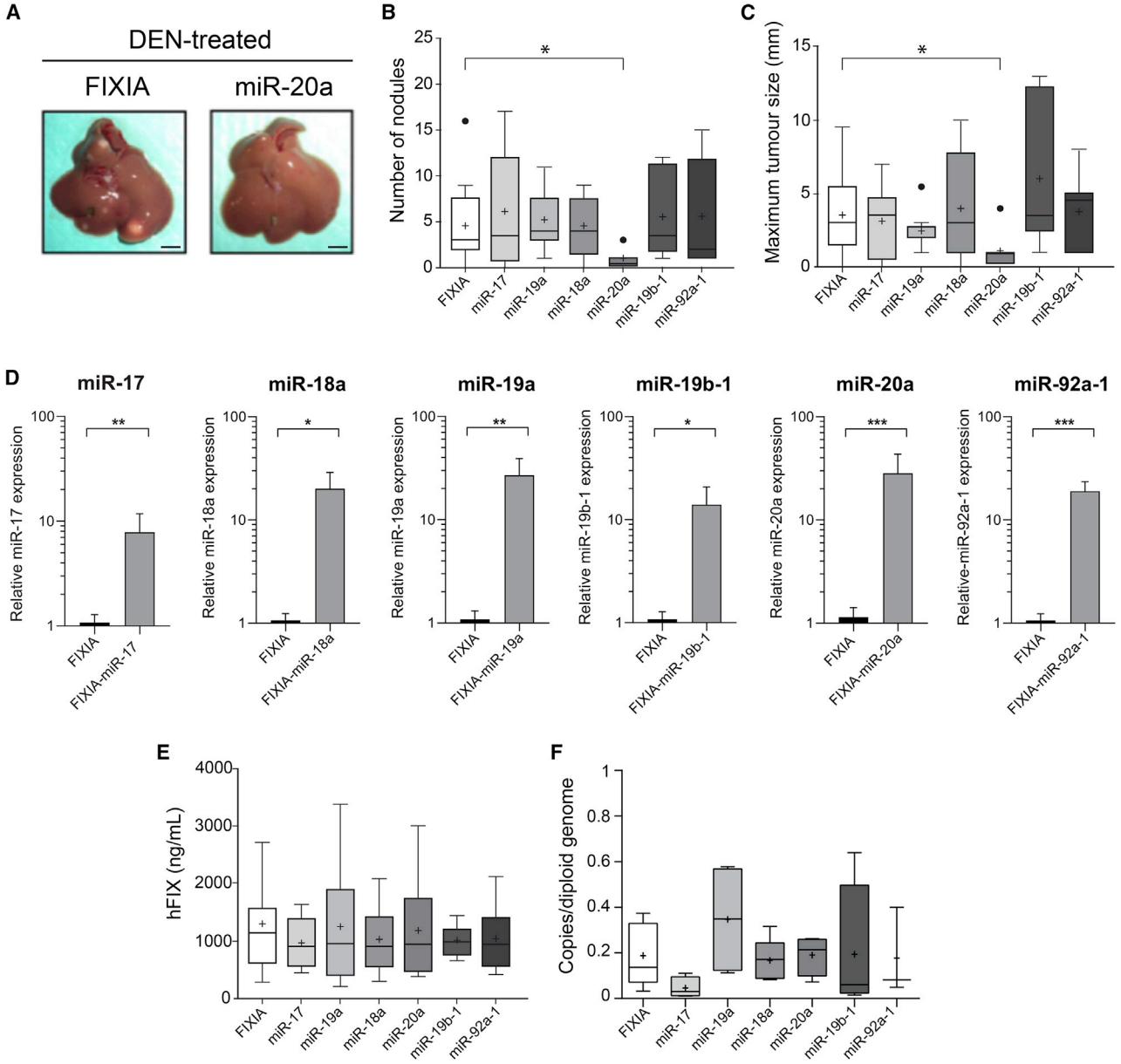

Figure 3. Evaluation of the *miR-17-92* Cluster on Hepatocarcinogenesis in a DEN-Induced Mouse Model

C57BL/6JRj male mice were subjected to a pre-weaning protocol of diethylnitrosamine (DEN) initiation. DEN (12.5 mg/kg) was injected intraperitoneally in 14-day-old mice. Then, at 4 weeks post-injection, mice were hydrodynamically transfected with 10 μg of either the *PB-hFIXIA-miR* or *PB-hFIXIA* construct and 2 μg of PB transposase-encoding plasmid (*PB-hFIXIA*, n = 17 mice; *PB-hFIXIA-miR-17*, n = 8 mice; *PB-hFIXIA-miR-19a*, n = 9 mice; *PB-hFIXIA-miR-18a*, n = 9 mice; *PB-hFIXIA-miR-20a*, n = 8 mice; *PB-hFIXIA-miR-19b-1*, n = 6 mice; *PB-hFIXIA-miR-92a-1*, n = 8 mice). After 36 weeks of DEN initiation, mouse livers were assessed to compare the tumor burden among the different treatments. (A) Macroscopic tumor burden. Scale bars represent 5 mm. (B) Number of tumor nodules. Graph presents the mean ± SEM of data obtained from individual mice; two-tailed unpaired Student's t test (n.s., not significant; *$p < 0.05$, **$p < 0.01$) (*PB-hFIXIA*, n = 17 mice; *PB-hFIXIA-miR-17*, n = 8 mice; *PB-hFIXIA-miR-19a*, n = 9 mice; *PB-hFIXIA-miR-18a*, n = 9 mice; *PB-hFIXIA-miR-20a*, n = 8 mice; *PB-hFIXIA-miR-19b-1*, n = 6 mice; *PB-hFIXIA-miR-92a-1*, n = 8 mice). (C) Maximum size of tumor nodules. Graph presents the mean ± SEM of data obtained from individual mice; two-tailed unpaired Student's t test (n.s., not significant; *$p < 0.05$, **$p < 0.01$) (*PB-hFIXIA*, n = 17 mice; *PB-hFIXIA-miR-17*, n = 8 mice; *PB-hFIXIA-miR-19a*, n = 9 mice; *PB-hFIXIA-miR-18a*, n = 9 mice; *PB-hFIXIA-miR-20a*, n = 8 mice; *PB-hFIXIA-miR-19b-1*, n = 6 mice; *PB-hFIXIA-miR-92a-1*, n = 8 mice). (D) Quantitative miR expression levels in the mouse liver at 36 weeks post-treatment measured by qPCR to assess the elevated selected miR expression in hFIXIA-*miRs*-treated mice. Graph represents the mean ± SEM of data obtained from individual mice; two-tailed unpaired Student's t test (n.s., not significant; *$p < 0.05$, **$p < 0.01$) (*PB-hFIXIA*, n = 5 mice; *PB-hFIXIA-miR-17*, n = 3 mice; *PB-hFIXIA-miR-19a*, n = 4 mice; *PB-hFIXIA-miR-18a*, n = 5 mice;

(legend continued on next page)

liver tissues of *PB-HRAS^{G12V}/PB-c-MYC*-transfected mice, consistent with the presence of hepatic tumor lesion and large vacuoles in the tumor area (Figure 4C, left panel, black solid arrow). Consistently, a marked accumulation of lipid content was present in the vacuolated region within the liver tumor of *PB-HRAS^{G12V}/PB-c-MYC*-transfected mice (Figure 4C, right panel, black dotted arrow; also see Figure 3E). *PB-HRAS^{G12V}/PB-c-MYC*-transfected mice showed an increase of hepatic fibrosis in liver tissues compared to other groups (Figure 4C, middle panel; also see Figure 3F). In particular, the histological features of hepatocytes with ballooning degeneration (Figure 4D, upper panel), Mallory-Denk bodies (Figure 4D, upper panel), and infiltrating inflammatory cells (Figure 4D, middle panel) were uniquely identified in *PB-HRAS^{G12V}/PB-c-MYC*-transfected group. Collectively, this indicates that *HRAS^{G12V}/c-MYC*-induced liver tumors displayed the typical characteristics of steatohepatitic HCC (SH-HCC).[45,46]

Molecular Analysis of RNA Expression Profiles and Pathway Analysis during *HRAS^{G12V}/c-MYC*-Mediated Hepatocarcinogenesis

To better characterize the rapid-onset HCC model and gain better insights into the molecular interplays between *HRAS^{G12V}* and *c-MYC* to induce HCC development in mice, we conducted a more comprehensive RNA expression profile study of 95 selected genes that are known to associate with liver cancer using qRT-PCR (Table S4). Subsequently, the gene expression levels from the *PB-HRAS^{G12V}/PB-c-MYC*-transfected cohort were compared with those from the non-injected control to identify differentially expressed genes (DEGs). Of those 95 genes associated with liver cancer, the expression pattern of 14 DEGs (13 upregulated genes and 1 downregulated gene) was distinctly observed only in the *PB-HRAS^{G12V}/PB-c-MYC*-transfected cohort versus the non-injected controls (Figures 5A and 5B). Among the 14 DEGs, *Aurka*, *Cdc20*, and *Igf2* exhibited a marked upregulation (i.e., 137-fold, 262-fold, and 1,034-fold change, respectively). In contrast, in the *PB-HRAS^{G12V}*-transfected cohort, there were three DEGs compared to the non-injected control (i.e., *Egf*, *Stm1*, and *Igf2*) (Figures 5A and 5B). In the *PB-c-MYC*-transfected cohorts, there were seven DEGs compared to the non-injected control (i.e., *Adam17*, *Birc2*, *Epo4*, *Pdgfra*, *Akt1*, *Cdkn1a*, and *Rb1*) (Figures 5A and 5B).

Next, a protein-protein interaction (PPI) network of the 14 DEGs, HRAS^{G12V}, and c-MYC was generated using STRING software to better understand how these proteins systemically interacted during hepatocarcinogenesis. The constructed PPI network was highly connected and non-random (clustering coefficient = 0.771, PPI enrichment p = 9.55e−13) with an average node degree of 4.25 (Figure 5C). Notably, Aurka, Akt, and Trp53 exhibited a relatively greater number of interactions (node degree = 6, 13, and 14, respectively) than the average. Taken together, this suggests that Aurka, Akt, and Trp53 may play a crucial role in *HRAS^{G12V}*- and *c-MYC*-dependent hepatocarcinogenesis.[47–49] We further explored the biological significances of 14 DEGs using Profiler software for Gene Ontology (GO) and Kyoto Encyclopedia of Genes and Genomes (KEGG) pathway enrichment analyses. The results obtained from GO analysis showed that the DEGs were significantly involved with regulation of cell cycle (9–11/14 DEGs), apoptotic (11/14 DEGs), and metabolic processes (11–13/14 DEGs) (Table S1). Similarly, significant biological pathways of the DEGs based on KEGG pathway enrichment consist of pathways involved in apoptosis (6/14 DEGs), cellular senescence (5/14 DEGs), p53 signaling (4/14 DEGs), and cell cycle (4/14 DEGs) (Table S1).

Long-Term Follow-Up of Tumor Progression in Rapid-Onset HCC Model

To better characterize the disease onset and tissue-specific tumorigenesis of the HCC model using the hepatocyte-specific hyPB platform, a long-term follow-up study was carried out in mice stably transfected with *PB-HRAS^{G12V}* in combination with *PB-c-MYC* or with either the *PB-HRAS^{G12V}* or *PB-c-MYC* transposon plasmid alone. These PB transposons were co-transfected with an expression construct encoding the hyperactive PB transposase to enable the efficient stable integration and expression of *HRAS^{G12V}* and/or *c-MYC* in the transfected hepatocytes. Kaplan-Meier survival analysis revealed that the median survival of *PB-HRAS^{G12V}/PB-c-MYC*-transfected mice was 93 days, which was 2.6-fold faster than that of mice transfected with only *PB-HRAS^{G12V}* (Figure 6A). In contrast, mice stably transfected with *PB-c-MYC*, *PB-hFIXIA*, or PBS survived for 365 days (Figure 6A), at which time the experiment was terminated. The decrease in median survival observed in *PB-HRAS^{G12V}/PB-c-MYC*-transfected mice was consistent with rapid HCC development and/or progression, including early-onset tumorigenesis and massive HCC tumor growth, compared to those in the other cohorts (Figure 6B). In particular, hepatocarcinogenesis progressed more rapidly in *PB-HRAS^{G12V}/PB-c-MYC*-overexpressing mice than in DEN-treated mice (Figure 6A). Tumorigenesis was restricted to the liver and absent in other organs and tissues, consistent with the use of the hepatocyte-specific *HS-CRM8-TTR$_{min}$* promoter to drive the expression of *HRAS^{G12V}* and *c-MYC* (Figure 6B). The elevated expression of the proliferation marker protein Ki-67 (*Mki67*) gene, one of the most common

PB-hFIXIA-miR-20a, n = 4 mice; *PB-hFIXIA-miR-19b-1*, n = 4 mice; *PB-hFIXIA-miR-92a-1*, n = 3 mice). (E) Quantitative hFIX protein expression levels at 36 weeks post-treatment measured by ELISA to monitor the transfection efficiency of PB transposons. Graph represents the mean ± SEM of data obtained from individual mice; two-tailed unpaired Student's t test (n.s., not significant; *p < 0.05, **p < 0.01) (*PB-hFIXIA*, n = 17 mice; *PB-hFIXIA-miR-17*, n = 8 mice; *PB-hFIXIA-miR-19a*, n = 9 mice; *PB-hFIXIA-miR-18a*, n = 9 mice; *PB-hFIXIA-miR-20a*, n = 8 mice; *PB-hFIXIA-miR-19b-1*, n = 6 mice; *PB-hFIXIA-miR-92a-1*, n = 8 mice). (F) Quantitative PB transposon copy number per diploid genome in the mouse liver at 36 weeks post-treatment measured by qPCR to confirm the presence of the PB transposon in mouse hepatocytes after transfection. Graph represents the mean ± SEM of data obtained from individual mice; two-tailed unpaired Student's t test (n.s., not significant; *p < 0.05, **p < 0.01) (*PB-hFIXIA*, n = 5 mice; *PB-hFIXIA-miR-17*, n = 4 mice; *PB-hFIXIA-miR-19a*, n = 4 mice; *PB-hFIXIA-miR-18a*, n = 5 mice; *PB-hFIXIA-miR-20a*, n = 4 mice; *PB-hFIXIA-miR-19b-1*, n = 4 mice; *PB-hFIXIA-miR-92a-1*, n = 3 mice).

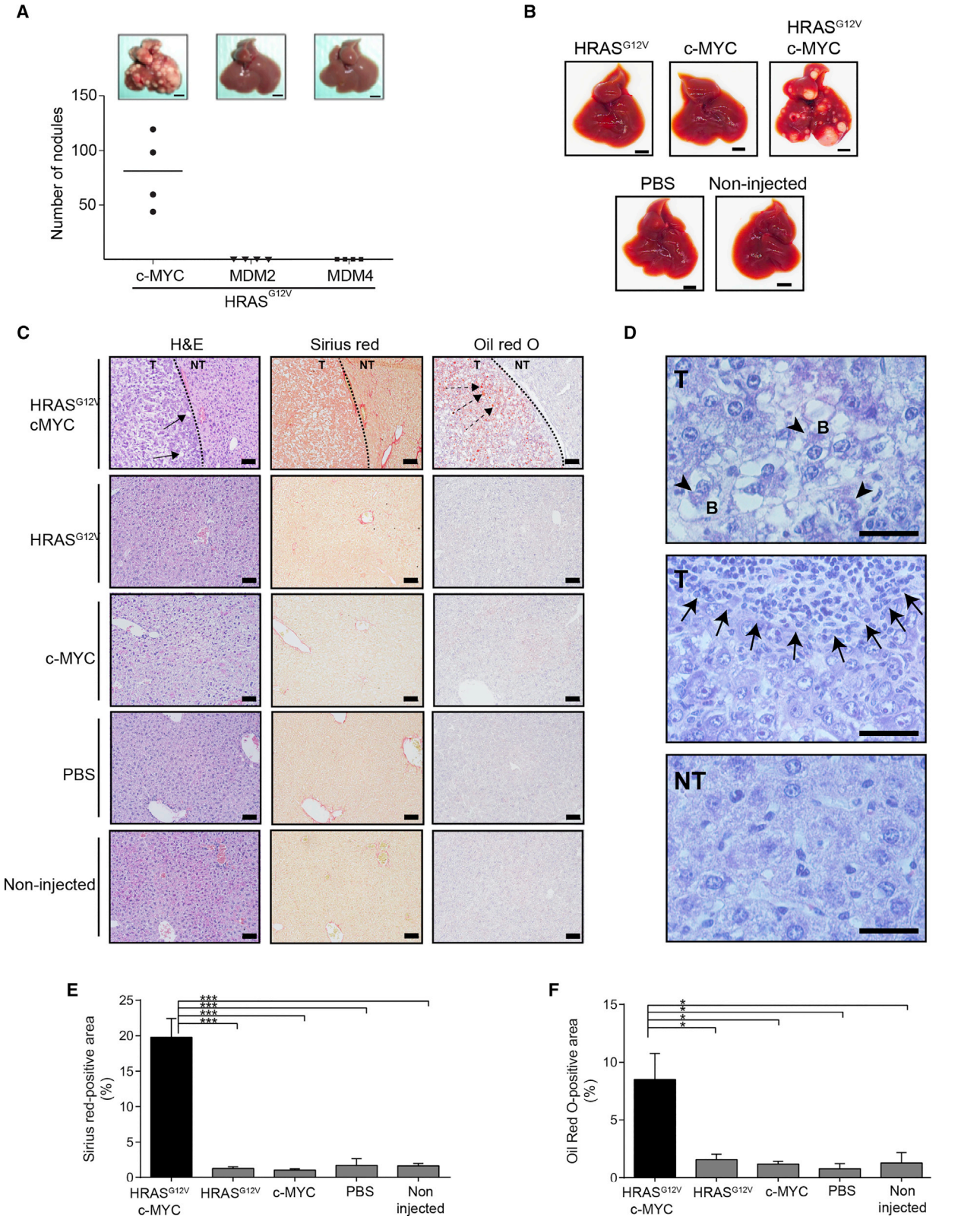

(legend on next page)

proliferative markers in HCC, was clearly observed in *HRAS*^{G12V} and *c-MYC* liver tissues (Figure 6C).[50–52] In addition, we identified a dysregulation of other biomarkers (i.e., *GluI*, *Hadha* [hydroxyacyl-coenzyme A dehydrogenase trifunctional multienzyme complex subunit alpha], *Acly* [ATP-citrate synthase], *Sc1*, and *Fasn* [fatty acid synthase]) in *HRAS*^{G12V}/*c-MYC* liver tissues, which were known to be associated with *HRAS*^{G12V} and *c-MYC*-induced hepatic tumors (Figure 6C).[50] RNA expression analysis confirmed that only the mice transfected with *PB*-c-*MYC*/*PB-HRAS*^{G12V} expressed high levels of both *HRAS* and *c-MYC* mRNA (Figure 6D). In contrast, control mice transfected with either the *PB-HRAS*^{G12V} or *PB-c-MYC* transposon only expressed increased levels of *HRAS*^{G12V} or *c-MYC* mRNA, respectively (Figure 6D). The long-term presence of the *HRAS*^{G12V} or *c-MYC* transgene in transfected livers is consistent with the stable genomic integration of the PB transposon responsible for the long-term *HRAS*^{G12V} or *c-MYC* mRNA expression (Figure 6E). Notably, an increase of copy number of PB transposon was observed in liver tumor compared to non-tumor liver tissue in the *HRAS*^{G12V}/*c-MYC* group (Figure 6F). In conclusion, we established a rapid-onset HCC model following the hepatocyte-specific delivery and expression of the *HRAS*^{G12V} and *c-MYC* oncogenes in adult mouse livers using the hyPB platform. These results indicate that the *HRAS*^{G12V} and *c-MYC* oncogenes cooperate in the development and/or progression of HCC.

miR-20a Suppresses Tumorigenesis in the Rapid-Onset HCC Model

To assess the robustness of the tumor suppressor effects of *miR-20a*, which were initially validated in the slow-onset chemically induced HCC model (Figure 3), we subsequently explored whether *miR-20a* could also function to suppress HCC initiation in the more aggressive, rapid-onset *HRAS*^{G12V}/*c-MYC* HCC model. Ultimately, this would provide more comprehensive insight into the inhibitory roles of *miR-20a* not only on tumor progression but also tumor initiation. HCC formation was induced by the liver-directed transfection of *PB-HRAS*^{G12V} and *PB-c-MYC* in C57BL/6JRj male mice in conjunction with a plasmid encoding a hyperactive PB transposase. The recipient mice were also transfected in parallel either with the *PB-hFIXIA-miR-20a* transposon or its corresponding *PB-hFIXIA* control. Consistent with the results obtained in the chemically induced HCC model, a significant reduction in HCC tumor formation was apparent in the HCC mice transfected with the *PB-hFIXIA-miR-20a* transposon compared to that in the *PB-hFIXIA* control group (Figure 7A). Macroscopic liver examination did not reveal any HCC formation in any cohort at 3 weeks post-transfection. Although all mice developed HCC at 6 weeks post-transfection (Figure 7A), a relatively robust and significant 4-fold reduction in HCC tumor nodules was apparent in the *PB-hFIXIA-miR-20a*-transfected livers compared to that in the controls (Figure 7B). Moreover, *miR-20a* overexpression in HCC mice following *PB-hFIXIA-miR-20a* transfection significantly prolonged their overall survival for at least 140 days, whereas the median survival of the control group was only 85 days (Figure 7C). This is consistent with a significantly 44-fold higher *miR-20a* expression in *PB-hFIXIA-miR-20a*-transfected HCC mice compared to the control *PB-hFIXIA* group (Figure 7D). In the liver tissues of the *PB-hFIXIA-miR-20a*-transfected HCC group, a marked 4-fold increase of *miR-20a* expression level in non-tumor area compared to tumor area was observed (Figure 7E). In addition, the copy numbers of all three PB transposons (i.e., *PB-HRAS*^{G12V}, *PB-c-MYC*, and *PB-hFIXIA-miR-20a*) present in non-tumor region *PB-hFIXIA-miR-20a*-transfected livers were comparable, suggesting at least 40% of overall transfection efficiency of each PB transposon (Figure 7F). FIX levels (Figure 7G) and transposon copy number (Figure 7H) were not significantly different between the *PB-hFIXIA-miR-20a*-transfected recipient mice and the *PB-hFIXIA*-transfected controls. These results confirm that *miR-20a* is a robust tumor suppressor gene capable of inhibiting HCC development even in a rapid-onset *HRAS*^{G12V}/*c-MYC* HCC model.

Figure 4. Establishment and Characterization of Rapid-Onset HCC Model

Six-week-old C57BL/6JRj male mice were hydrodynamically co-transfected with 1 μg of a single transposon encoding an oncogene (*PB-c-MYC*, *PB-MDM2*, or *PB-MDM4*) and *PB-HRAS*^{G12V} and 1 μg of hyperactive PB-encoding plasmid. As a control to study the effect of HRAS^{G12V} and c-MYC cooperation, mice were hydrodynamically co-transfected with 1 μg of single transposon plasmid expressing either *HRAS*^{G12V} or *c-MYC* (*PB-HRAS*^{G12V} or *PB-c-MYC*, respectively) and 1 μg of hyperactive PB-encoding plasmid. PBS-injected and non-injected mice were used as a negative control in this study. After 8 weeks of treatment, mouse livers were observed to compare the tumor burden among the different treatments. (A) Macroscopic tumor burden and number of tumor nodules from mice transfected with transposons expressing *HRAS*^{G12V} and *c-MYC* at 8 weeks post-injection. Graph presents the mean ± SEM of data obtained from individual mice; two-tailed unpaired Student's t test (n.s., not significant; *$p < 0.05$, **$p < 0.01$). Scale bars represent 5 mm (*PB-HRAS*^{G12V}+*PB-c-MYC*, n = 4 mice; *PB-HRAS*^{G12V}+*PB-MDM2*, n = 4 mice; *PB-HRAS*^{G12V}+*PB-MDM4*, n = 4 mice). (B) Macroscopic tumor burden from mice transfected with *PB-HRAS*^{G12V}+*PB-c-MYC*, *PB-HRAS*^{G12V}, *PB-c-MYC*, PBS, and without injection at 8 weeks post-injection. Scale bars represent 5 mm. (C) Microscopic representatives of mouse liver tissue sections stained with hematoxylin and eosin (left panel, original magnification, ×200), Sirius red (middle panel, original magnification, ×200), and oil red O (right panel, original magnification, ×200) to examine the presence of histopathology features of HCC, formation of liver fibrosis, and lipid droplet accumulation in mice transfected with *PB-HRAS*^{G12V}+*PB-c-MYC*, *PB-HRAS*^{G12V}, *PB-c-MYC*, PBS, and without injection. Scale bars represent 20 μm. Solid arrows indicated large empty vacuolated regions. Dotted arrow indicates lipid droplets (stained in red). Tumor (T) and non-tumor (NT) areas in liver tissue are divided using dotted lines. (D) Microscopic representatives of tumor (T, upper and middle panels) and non-tumor (NT, lower panel) areas of mouse liver tissue sections from *PB-HRAS*^{G12V}+*PB-c-MYC*-injected group stained with hematoxylin and eosin (original magnification, ×400). Black arrowhead indicates the presence of Mallory-Denk body. "B" indicates ballooned hepatocyte. Black arrow indicates an infiltration of inflammatory cells in liver tissue. (E) Percentages of sirius red-positive area in liver tissues from mice transfected with *PB-HRAS*^{G12V}+*PB-c-MYC*, *PB-HRAS*^{G12V}, *PB-c-MYC*, PBS, and without injection at 8 weeks post-injection. Graph presents the mean ± SEM of data obtained from individual mice; two-tailed unpaired Student's t test (***$p < 0.001$) (*PB-HRAS*^{G12V}+*PB-c-MYC*, n = 4 mice; *PB-HRAS*^{G12V}, n = 4 mice; *PB-c-MYC*, n = 4 mice; PBS-injected, n = 4 mice; non-injected, n = 4 mice). (F) Percentages of oil red O-positive area in liver tissues from mice transfected with *PB-HRAS*^{G12V}+*PB-c-MYC*, *PB-HRAS*^{G12V}, *PB-c-MYC*, PBS, and without injection at 8 weeks post-injection. Graph presents the mean ± SEM of data obtained from individual mice; two-tailed unpaired Student's t test (***$p < 0.001$) (*PB-HRAS*^{G12V}+*PB-c-MYC*, n = 4 mice; *PB-HRAS*^{G12V}, n = 4; *PB-c-MYC*, n = 4 mice; PBS-injected, n = 4 mice; non-injected, n = 4 mice).

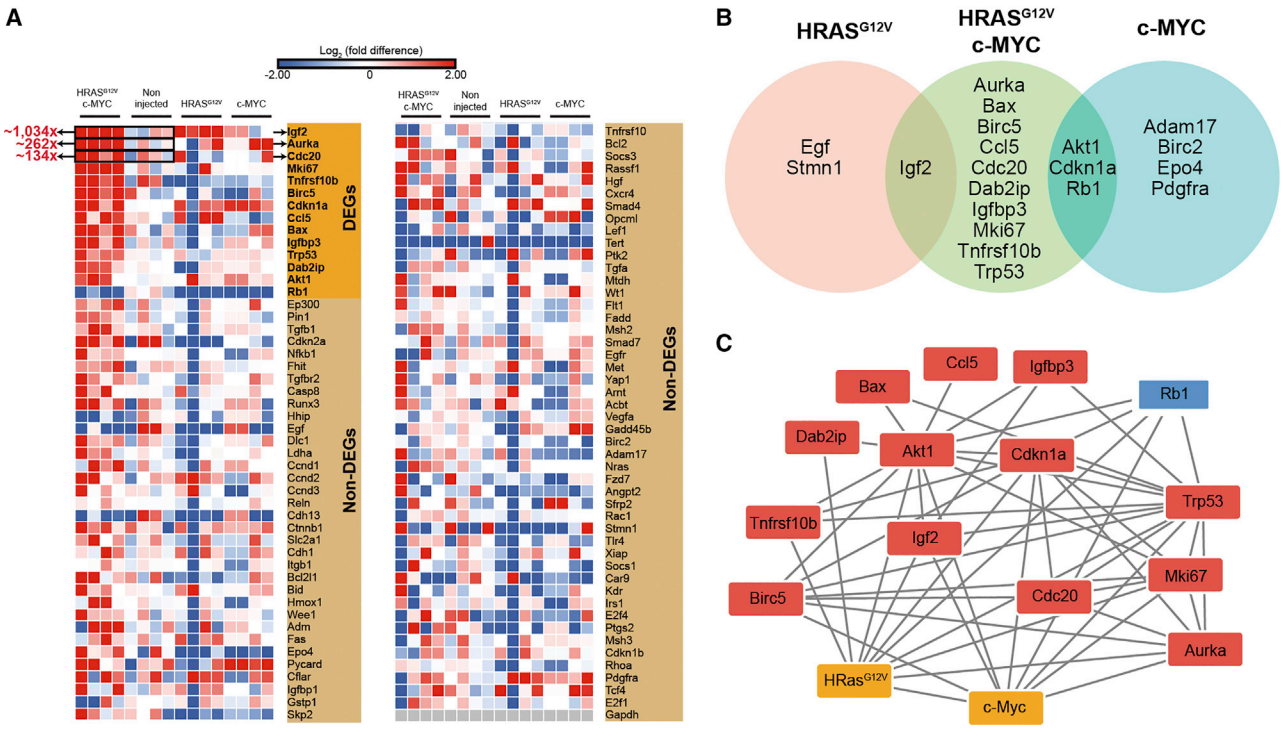

Figure 5. Molecular Analysis of RNA Expression Profiles and Pathway Analysis during *HRAS^{G12V}/c-MYC*-Mediated Hepatocarcinogenesis

Six-week-old C57BL/6JRj male mice were hydrodynamically co-transfected with 1 μg of *PB-c-MYC*, 1 μg of *PB-HRAS^{G12V}*, and 1 μg of hyperactive PB-encoding plasmid. As a control to study the cooperative effect of HRAS^{G12V} and c-MYC, mice were hydrodynamically co-transfected with 1 μg of single transposon plasmid expressing either HRAS^{G12V} or c-MYC (*PB-HRAS^{G12V}* or *PB-c-MYC*, respectively) and 1 μg of hyperactive PB-encoding plasmid. Non-injected mice were used as a negative control in this study. After 8 weeks of treatment, total extracted RNA from mouse liver tissues was used as a template for qRT-PCR using primers targeting 95 genes that are known to be associated with hepatocarcinogenesis. (A) Heatmap representing $\log_2$ fold change of all 95 gene expression profiles from *PB-HRAS^{G12V}+PB-c-MYC*, *PB-HRAS^{G12V}*, *PB-c-MYC*, and non-injected groups. Genes that showed $p < 0.05$ for differential expression were defined as differentially expressed genes (DEGs); otherwise, they were defined as non-differentially expressed genes (non-DEGs). Red and blue indicate upregulation and downregulation of the genes, respectively. DEGs were ranked based on fold difference (from high to low), and the number on the left of the heatmap indicates an average fold difference (*PB-HRAS^{G12V}+PB-c-MYC*, n = 4 mice; *PB-HRAS^{G12V}*, n = 4; *PB-c-MYC*, n = 4 mice; non-injected, n = 4 mice). (B) Venn diagram of DEGs in *PB-HRAS^{G12V}+PB-c-MYC*, *PB-HRAS^{G12V}*, and *PB-c-MYC* groups compared to non-injected groups. The genes in intersected areas were identified as common DEGs between groups whereas the genes in non-intersected areas indicated group-specific DEGs. (C) Protein-protein interaction (PPI) networks of all DEGs of *PB-HRAS^{G12V}+PB-c-MYC*-transfected group versus non-injected group generated by the STRING database (https://string-db.org).

Effects of *miR-20a* on Gene Expression Signatures in the Rapid-Onset HCC Model

We subsequently determined whether *miR-20a* altered the expression of any of the putative *miR-20a* target genes such as phosphatase and tensin homolog (*Pten*), Unc-51-like autophagy activating kinase 1 (*Ulk1*), and induced myeloid leukemia cell differentiation protein (*Mcl1*) (Table S5).[14,53–56] The effects of *miR-20a* overexpression on the expression at the post-transcriptional and translational levels of the putative target genes were examined. Interestingly, Pten expression, a known tumor suppressor gene in HCC, was significantly upregulated in *HRAS^{G12V}/c-MYC* HCC mice that were stably transfected with the *PB-hFIXIA-miR-20a* transposon to levels that were comparable to those in the control mice injected with PBS (Figures 7B, 7C, and 8A).[57,58] In contrast, no differential expression of *Pten* at the mRNA level was apparent (Figure S2D). This suggests that *miR-20a* potentially modulates Pten expression at the translational level during HCC suppression *in vivo* possibly through an as yet unknown indirect mechanism, potentially involving inhibition of a negative regulator of Pten. In contrast to Pten, overexpression of *miR-20a* following liver-directed transfection with *PB-hFIXIA-miR-20a* transposons affected neither RNA nor protein expression levels of the other putative *miR-20a* candidate targets (i.e., *Mcl1* and *Ulk1*; Figure S2).

To gain a better understanding of the possible tumor suppressor mechanisms of *miR-20a* in the rapid-onset *HRAS^{G12V}/c-MYC* HCC model, RNA expression profiling of the selected 95 liver cancer-related genes in mouse liver tissues of *PB-hFIXIA-miR-20a* and *PB-hFIXIA*-transfected cohorts was carried out using qRT-PCR (Table S4). We found that 14 genes were significantly dysregulated in the *hFIXIA-miR-20a* cohort versus *hFIXIA* controls (13 downregulated genes and 1 upregulated gene) (Figure 8D). Notably, the oncogene *Tgfa* and the tumor suppressor gene *Cdh13* showed a more pronounced differential expression pattern compared to other DEGs

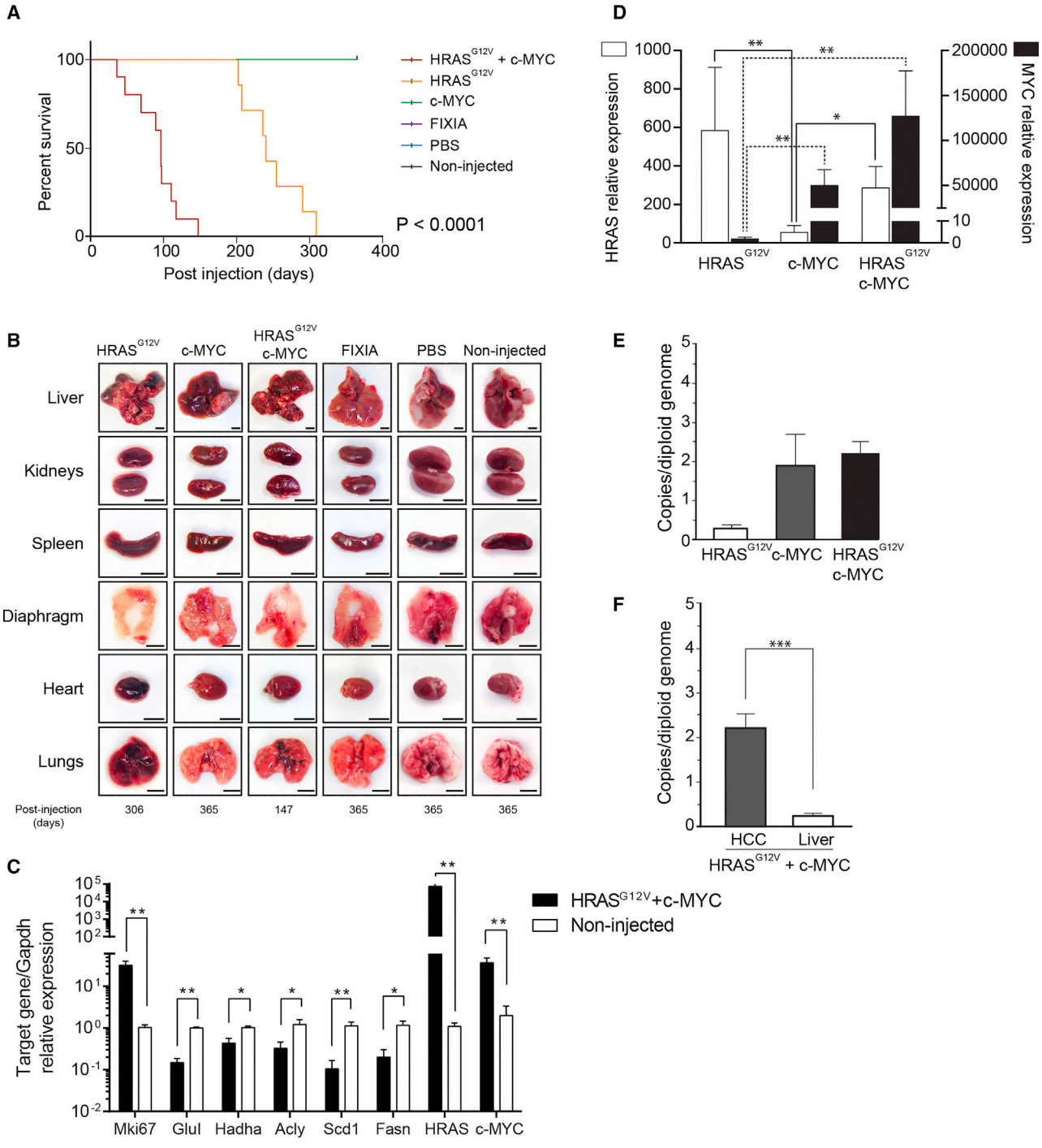

Figure 6. Long-Term Follow-Up of Tumor Progression in Rapid-Onset HCC Model

Six-week-old C57BL/6JRj male mice were hydrodynamically co-transfected with 1 μg of *PB-c-MYC* in combination with *PB-HRAS*^{G12V}, *PB-HRAS*^{G12V}, *PB-c-MYC*, or *PB-hFIXIA* and 1 μg of hyperactive PB-encoding plasmid. As controls, mice were injected with PBS. (A) One-year Kaplan-Meier survival curve analysis of treated mice from all groups. Graph presents survival days of individual mice; log-rank test (*PB-HRAS*^{G12V}+*PB-c-MYC*, n = 10 mice; *PB-HRAS*^{G12V}, n = 7 mice; *PB-c-MYC*, n = 7 mice; *PB-hFIXIA*, n = 7 mice; PBS-injected, n = 7 mice). (B) Representative macroscopic morphology of mouse organs from all groups. Tumor formation was only observed in mouse livers of the combined *PB-c-MYC* and *PB-HRAS*^{G12V} and individual *PB-HRAS*^{G12V} treatment groups at different onset periods. Scale bars represent 5 mm. (C) Relative mRNA expression of a proliferative gene marker (i.e., *Mki67*) and other genes that are responsible for glutamine metabolism (i.e., *Glul*) and fatty acid metabolism (i.e., *Hadha*, *Acly*, *Scd1* [stearoyl-coenzyme A desaturase 1], and *Fasn*) from the combined *PB-c-MYC* and *PB-HRAS*^{G12V} and healthy (non-injected) groups. Graph presents the mean ± SEM

(legend continued on next page)

(i.e., 20-fold downregulation and 86-fold upregulation, respectively). The PPI network of 14 DEGs from the *hFIXIA-miR-20a* cohort versus *hFIXIA* control (clustering coefficient = 0.51, PPI enrichment p = 1.67e−09, average node degree = 2.43) showed that BCL2-like 1 (Bcl2l1) exhibited the highest number of interactions among other genes (six interactions), suggesting its central role during *miR-20a*-mediated HCC suppression in mice (Figure 8E). These DEGs were functionally enriched in genes involved in the regulation of apoptotic processes (12/14 DEGs), programmed cell death (12/14 DEGs), and cell cycle (10/14 DEGs) based on GO analysis (Table S2). Correspondingly, functional pathway enrichment of all DEGs using the KEGG database includes pathways involved in apoptosis (5/14 DEGs), cellular senescence (4/14 DEGs), and other signaling pathways (i.e., nuclear factor κB [NF-κB] signaling pathway, 4/14 DEGs and TNF signaling pathway, 4/14 DEGs) that are known to be associated with cell death and apoptosis.[59,60]

DISCUSSION

In the current study, we validated a semi-high-throughput *in vivo* screen based on the hyPB transposon platform specifically designed to selectively express *miR*s in hepatocytes and identify those that affect HCC development and progression. We systematically analyzed the impact of each *miR* in the *miR-17-92* cluster (i.e., *miR-17*, *miR-18a*, *miR-19a*, *miR-20a*, *miR-19b-1*, and *miR-92*a-1) and other *miR*s that are thought to play a role in HCC (i.e., *miR-370*, *miR-1188*, *miR-341*, *miR-221*, *miR-222*, *miR-106b*, *miR-25*, *miR-93*, and *miR-106b*). Notably, the screening revealed that *miR-20a* functions as a tumor suppressor gene inhibiting HCC development and progression in both the slow-onset chemically induced and rapid-onset mouse models, which had not been shown previously. Our results indicated that *miR-20a* overexpression in the liver significantly decreased the number and expansion of HCC nodules, consistent with the significant prolongation of overall survival in the rapid-onset HCC model. For the chemically induced DEN HCC model, the *PB-hFIXIA-miR* transposons were transfected into the mice, 4 weeks after tumor initiation by chemical induction. Hence, the *miR-20a* likely suppressed tumor progression rather than tumor initiation per se since the tumors had already been initiated by DEN, 4 weeks prior to *miR-20a* overexpression. The DEN HCC model depends on the stochastic and random mutations that contribute to the subsequent initiation (and progression) of HCC. Typically, *Hras*, *Braf*, *Egfr*, and/or *Apc* genes are thought to play a role in DEN-induced hepatocellular carcinogenesis.[61] Consequently, this process is far less controllable and typically takes much longer for HCC tumors to develop (>9 months). In the rapid-onset HCC model, the PB transposons encoding $HRAS^{G12V}$/*c-MYC* and *miR-20a* were all injected at the same, implying that the *miR-20a* may also have an impact on tumor initiation per se in this model, although a possible effect on tumor progression cannot be excluded. The rationale for testing the effect of *miR-20a* in a rapid-onset model was to evaluate the impact of *miR-20a* in hepatocytes that from the onset already expressed high levels of *HRAS* and *c-MYC* oncogenes that synergistically contribute to HCC initiation and/or progression and that are therefore poised to rapidly progress toward full-blown HCC tumors. The demonstration that *miR-20a* can even suppress HCC tumors in such an aggressive, rapid-onset model as compared to a slow-onset model strongly suggests that *miR-20a* is a relatively potent tumor suppressor gene. Moreover, it shows that *miR-20a* can suppress HCC regardless of the method or mechanism of HCC initiation. This indicates that the tumor suppressor effects of *miR-20a* are not restricted to a single HCC model and suggests its therapeutic potential and broad implications for HCC in general.

To our knowledge, this is the first *in vivo* demonstration that *miR-20a* is a possible tumor suppressor gene in HCC. This is consistent with previous *in vitro* studies in tumor cell lines indicating that *miR-20a* inhibits cell proliferation and invasion and promotes cancer cell sensitization to apoptosis.[14,15,62] Moreover, *miR-20a* expression is downregulated in HCC samples from patients compared to that in normal tissue.[14,15,62] However, the biological significance of these previous observations was unknown. Our current study now establishes a direct causal link between *miR-20a* overexpression and suppression of HCC in *in vivo* models. The previous publications were based on *in vitro* studies in hepatic cell lines only or patient biopsies were circumstantial at best and never formally demonstrated based on *in vivo* HCC models that *miR-20a* is a tumor suppressor gene.[14,15] These previous studies merely showed differential *miR-20a* expression levels between normal and tumor cells, which does not formally establish a causal link between elevated *miR-20a* expression and tumor suppression in HCC *in vivo*. In fact, with the exception of *miR-20a*, we demonstrated that other candidate *miR* genes that were previously found to be differentially expressed in HCC compared to normal hepatocytes had no impact whatsoever on the HCC tumor initiation and/or progression *in vivo* (Figure 3; Figure S1).[13,16,17,19–22] Hence, our current findings caution against merely relying on *in vitro* data, which are prone to false positives and negatives, or patient biopsies, which do not formally establish a causal relationship between mi-R20a expression and HCC suppression. This

of data obtained from individual mice; Mann-Whitney U test (n.s., not significant; *p < 0.05, **p < 0.01) (*PB-c-MYC*+*PB-HRAS*^{G12V}, n = 5 mice; healthy (non-injected), n = 5 mice). (D) RNA expression analysis of *HRAS* and *c-MYC* in mouse livers of the combined *PB-c-MYC* and *PB-HRAS*^{G12V}, individual *PB-HRAS*^{G12V}, and *PB-c-MYC* treatment groups to determine the elevated oncogene expression according to the types of transfected oncogenes. Graph presents the mean ± SEM of data obtained from individual mice; Mann-Whitney U test (n.s., not significant; *p < 0.05, **p < 0.01) (Healthy (non-injected), n = 5 mice; *PB-c-MYC*+*PB-HRAS*^{G12V}, n = 6 mice; *PB-HRAS*^{G12V}, n = 6 mice; *PB-c-MYC*, n = 6 mice). (E) Quantitative PB transposon copy number per diploid genome in the mouse livers of the combined *PB-c-MYC* and *PB-HRAS*^{G12V}, individual *PB-HRAS*^{G12V}, and *PB-c-MYC* groups measured by qPCR to ensure the presence of the PB transposon in mouse hepatocytes after transfection. Graph presents the mean ± SEM of data obtained from individual mice; Mann-Whitney U test (n.s., not significant) (*PB-c-MYC*+*PB-HRAS*^{G12V}, n = 6 mice; *PB-HRAS*^{G12V}, n = 6 mice; *PB-c-MYC*, n = 6 mice).(F) Quantitative PB transposon copy number per diploid genome in the HCC tissue and normal liver tissue of combined *PB-c-MYC* and *PB-HRAS*^{G12V} mice measured by qPCR. Graph presents the mean ± SEM of data obtained from individual mice; Mann-Whitney U test (***P < 0.001). (n = 4 tissue samples of HCC regions and corresponding adjacent normal regions from 4 individual *PB-c-MYC*+*PB-HRAS*^{G12V}mice).

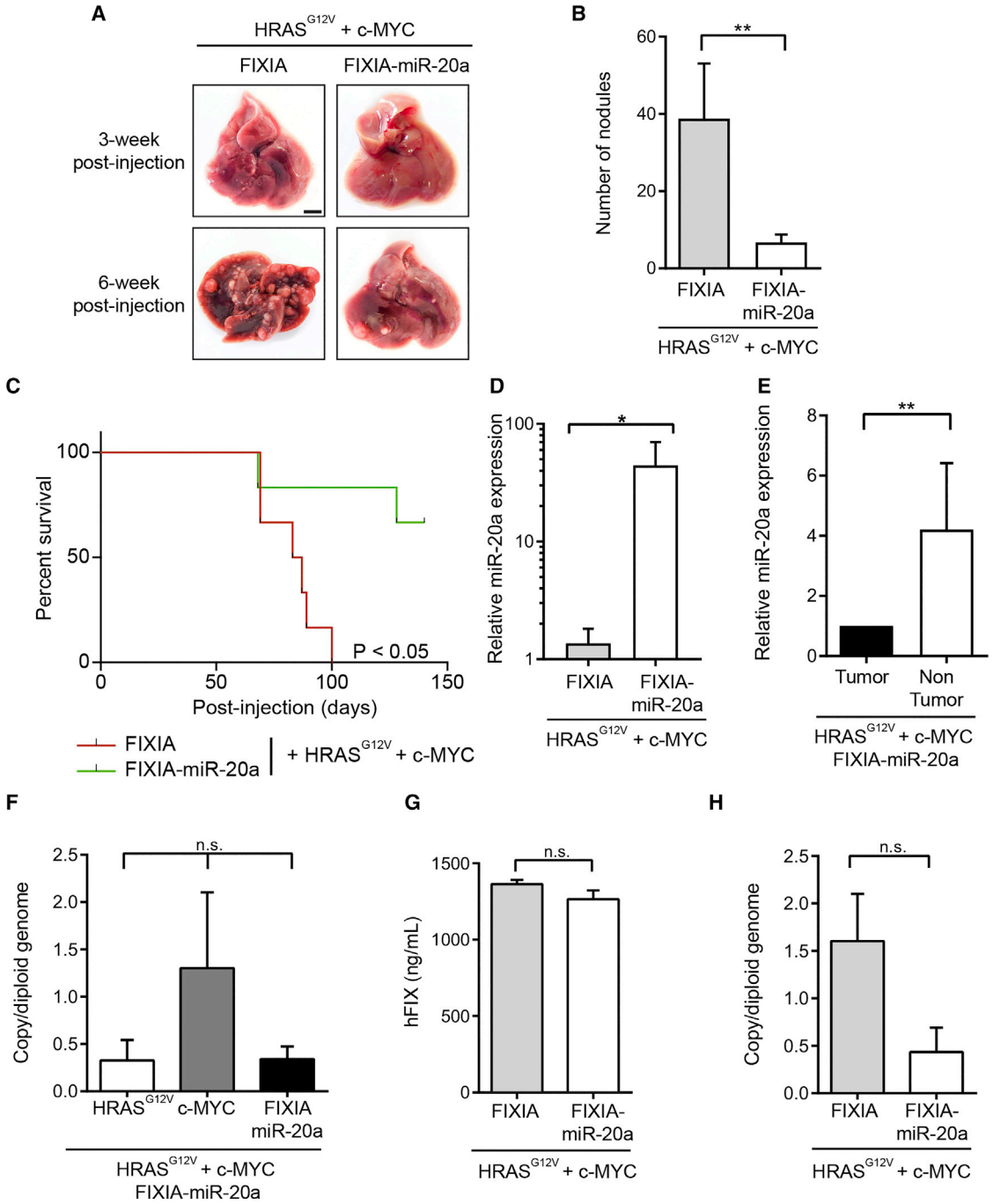

Figure 7. Analysis of the Tumor-Suppressive Effects of *miR-20a* in the Rapid-Onset HCC Model

Six-week-old C57BL/6JRj male mice were hydrodynamically co-transfected with (1) 0.25 μg of *PB-c-MYC*, (2) 0.25 μg of *PB-HRAS*^{G12V}, (3) 10 μg of either *PB-hFXIA* or *PB-hFIXIA-miR-20a*, and (4) 2.25 μg of hyperactive PB-encoding plasmid (*PB-hFIXIA*, n = 8 mice; *PB-hFIXIA-miR-20a*, n = 7 mice). (A) Representative macroscopic tumor burden was assessed at 3 and 6 weeks post-injection. Scale bars represent 5 mm. (B) Number of tumor nodules was counted at 6 weeks after injection to compare the hepatic tumor burden. Graph represents the mean ± SEM of data obtained from individual mice; Mann-Whitney U test (n.s., not significant; *$p < 0.05$, **$p < 0.01$) (*PB-hFIXIA*, n = 8 mice; *PB-hFIXIA-miR-20a*, n = 7 mice). (C) Kaplan-Meier survival curve analysis of *PB-hFIXIA* and *PB-hFIXIA-miR-20a*-treated HCC mice. Graph presents survival days of individual mice; log-rank test (*PB-hFIXIA*, n = 8 mice; *PB-hFIXIA-miR-20a*, n = 7 mice) (*PB-hFIXIA*, n = 6 mice; *PB-hFIXIA-miR-20a*, n = 6 mice). (D) Quantitative *miR-20a* expression in the liver tissues of *PB-hFIXIA-miR-20a-* and *PB-hFIXIA*-treated HCC groups at 6 weeks post-treatment measured by qRT-PCR. Graph represents the mean ± SEM of data obtained from individual mice; Mann-Whitney U test (*$p < 0.05$) (*PB-hFIXIA*, n = 5 mice; *PB-hFIXIA-miR-20a*, n = 5 mice). (E) Quantitative *miR-20a* expression in the tumor and

(legend continued on next page)

emphasizes the need for *in vivo* confirmation to assess the real impact of a given *miR* on tumor initiation/progression in HCC models.

We demonstrated that *miR-20a* altered the mRNA expression levels of several HCC-related genes in the *HRAS^{G12V}/c-MYC*-induced HCC mode, suggesting that each of them could play a role in HCC suppression by *miR-20a*. Notably, most of these differentially expressed genes were shown to functionally interact with *Bcl2l1*, which is itself also differentially expressed upon *miR-20a* overexpression. The *Bcl2l1* oncogene belongs to the Bcl-2 family, which exhibits anti-apoptotic activity through sequestration of BH3 domain-only molecules from Bak activation during apoptosis.[63] In addition, overexpression of *Bcl2l1* was observed in liver tissues of HCC patients and resulted in tumor progression.[64,65] This is consistent with downregulation of the *Bcl2l1* oncogene and reduction of HCC tumor burden following *PB-hFIXIA-miR-20a* transfection in the rapid-onset *HRAS^{G12V}/c-MYC*-induced HCC model. Alternatively, a significant upregulation of the *Cdh13* tumor suppressor gene and downregulation of the *Tgfa* oncogene may also have contributed to HCC suppression by *miR-20a* overexpression through inhibition of cell proliferation in liver.[66,67] Cdh13, a glycosylphosphatidylinositol (GPI)-anchored cadherin devoid of transmembrane and cytoplasmic domain, regulates hepatocyte function such as albumin secretion and urea synthesis. Interestingly, overexpression of *Cdh13* suppresses proliferation in gastric cancer cells.[68,69] Moreover, significant downregulation of *CDH13* expression was observed in liver tissues of patients with metastatic HCC.[66] *Tgfa* encodes transforming growth factor α (TGF-α) and binds to epidermal growth factor receptor and subsequently activates a signaling pathway that promotes cell proliferation.[70] Particularly in HCC, TGF-α enhances DNA synthesis and extracellular signal-regulated kinase (ERK)-mitogen-activated protein kinase (MAPK)-dependent cell proliferation. Moreover, TGF-α expression was upregulated in the liver of HCC patients.[71–74] Functional pathway enrichment analysis suggests that a *miR-20a*-mediated inhibitory mechanism may be associated with apoptotic processes, which are known to regulate HCC development.[75,76] Moreover, *miR-20a* may potentially suppress *HRAS^{G12V}/c-MYC*-mediated hepatocarcinogenesis by upregulating Pten protein expression levels, a known tumor suppressor gene in HCC.[77,78] Consistent with an increase of Pten protein expression following tumor regression in our study, previous findings showed that Pten protein deficiency promotes HCC development.[78,79] It is possible that indirect mechanisms account for the increase in Pten protein expression, for example through *miR-20a*-mediated inhibition of negative regulators of Pten, particularly since *miR-20a* overexpression did not affect the steady-state *Pten* mRNA levels. The prioritization of the 95 genes associated with HCC permitted identification of possible lead candidates that could play a key role in *miR-20a*-mediated hepatocarcinogenesis. However, it cannot be excluded that other genes may also play a role warranting future comprehensive transcriptomics and mechanistic studies, which are beyond the scope of the current study.

Previous studies have shown that the overexpression of short hairpin RNA (shRNA) can cause low-level hepatotoxicity that can facilitate the ability of the *c-MYC* oncogene to induce liver tumorigenesis.[80,81] Moreover, oversaturation of cellular microRNA/shRNA pathways may result in death, possibly by interfering with karyopherin exportin-5. However, the results of the present study suggest that enhanced tumorigenicity and/or hepatotoxicity may not be a concern for *miR-20a* overexpression because it diminishes tumorigenicity, even in the current rapid-onset HCC model that relies on the forced overexpression of the MYC and Ras oncogenes.

The tumor suppressor effect of *miR-20a* may not be restricted to HCC and may have broader implications for other types of malignancies. In particular, it was recently shown that *miR-20a* expression in liver sinusoidal endothelial cells (LSECs) inhibits colorectal metastasis to the liver.[82] Hence, to further assess the broader impact of *miR-20a* in oncology and confirm our current findings beyond HCC, future studies are needed to further investigate the role of *miR-20a* in cancers of different origins and different (sub)types. One of the main advantages of the current *in vivo* approach based on the selective hepatic overexpression of a given *miR* is that it allows the establishment of a causal relationship between *miR* expression and HCC, thus excluding possible unrelated associations. Interestingly, *miR-20a* was the only *miR* in the *miR-17-92* cluster that had an impact on HCC, challenging the prevailing assumption that *miR*s located in the *miR*-17-92 cluster typically function as oncogenes, as suggested by transgenic studies.[1,2,13,83]

In the current study, a rapid-onset HCC model was also developed to further validate and confirm the tumor suppressor properties of *miR-20a*. This rapid-onset HCC model was developed by the somatic and sustained overexpression of *HRAS^{G12V}* and *c-MYC* in hepatocytes following stable PB transposon-mediated genomic integration of the *HRAS^{G12V}* and *c-MYC* oncogenes. This rapid-onset model offers several advantages over conventional HCC models. The current rapid-onset HCC model is generated by co-delivery of *PB-c-MYC* and *PB-HRAS^{G12V}* and is based on the *de novo* expression in adult, post-mitotic hepatocytes, complementing the shRNA/*c-MYC* model

non-tumor liver tissues of *PB-hFIXIA-miR-20a*-treated HCC group at 6 weeks post-treatment measured by qRT-PCR. Graph represents the mean ± SEM of data obtained from individual mice; Mann-Whitney U test (**$p < 0.01$) (n = 5 tissue samples of tumor and corresponding adjacent non-tumor regions from five individual *PB-hFIXIA-miR-20a*-treated mice). (F) Quantitative copy number of all PB transposons (i.e., *PB-HRAS^{G12V}*, *PB-c-MYC*, and *PB-hFIXIA-miR-20a*) per diploid genome in the mouse liver of the *PB-hFIXIA-miR-20a*-treated group at 6 weeks post-treatment measured by qPCR. Graph represents the mean ± SEM of data obtained from individual mice; Mann-Whitney U test (n.s., not significant) (n = 5 mice). (G) Quantitative hFIX protein expression levels at 1 week post-treatment measured by ELISA to monitor the transfection efficiency of PB transposons. Graph represents the mean ± SEM of data obtained from individual mice; Mann-Whitney U test (n.s., not significant) (*PB-hFIXIA*, n = 6 mice; *PB-hFIXIA-miR-20a*, n = 6 mice). (H) Quantitative overall PB transposon copy number per diploid genome in the mouse liver at 6 weeks post-treatment measured by qPCR to confirm the presence of the PB transposon in mouse hepatocytes after transfection. Graph represents the mean ± SEM of data obtained from individual mice; Mann-Whitney U test (n.s., not significant) (*PB-hFIXIA*, n = 6 mice; *PB-hFIXIA-miR-20a*, n = 6 mice).

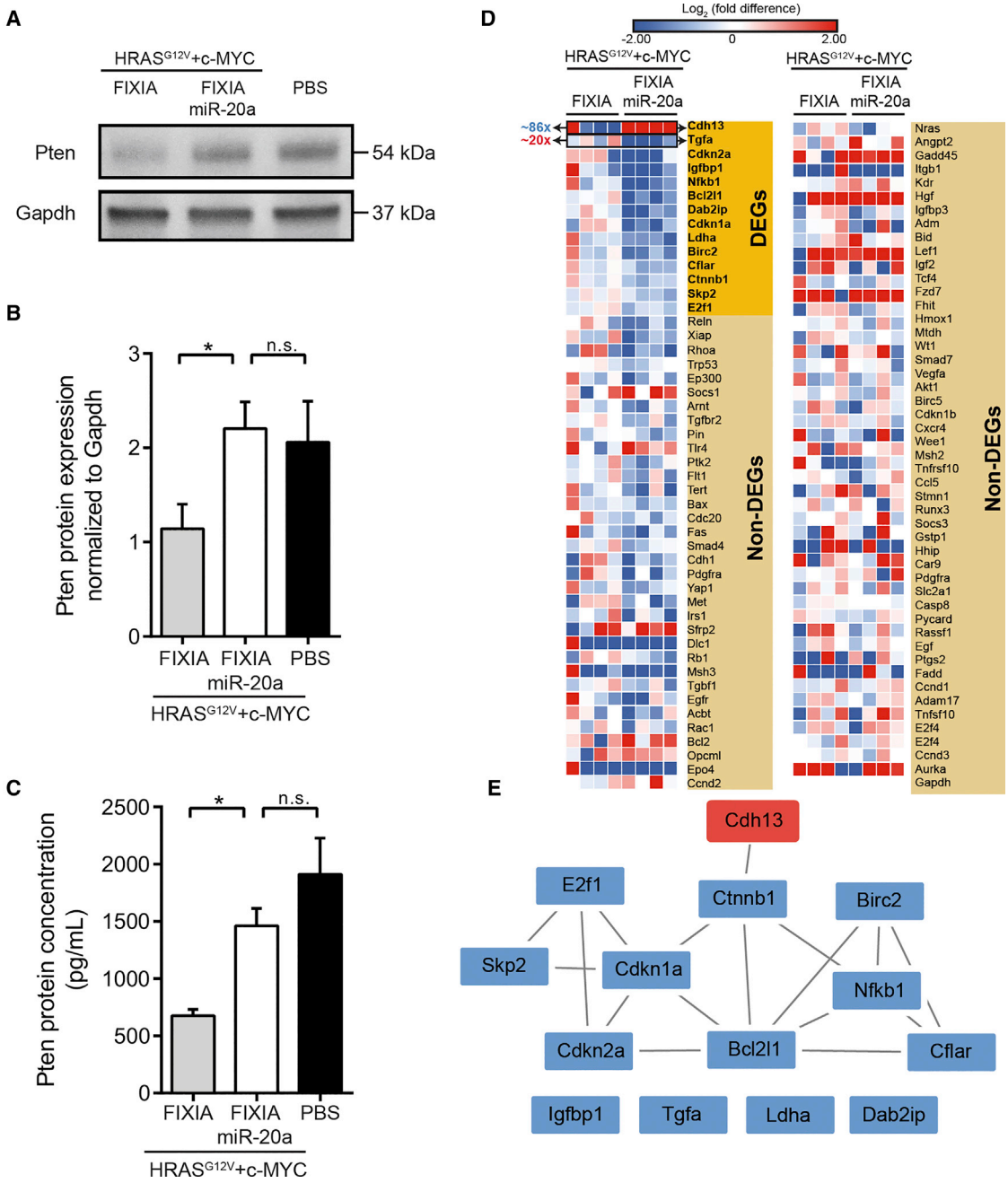

Figure 8. Effects of *miR-20a* on Gene Expression Signatures in the Rapid-Onset HCC Model

Six-week-old C57BL/6JRj male mice were hydrodynamically co-transfected with (1) 0.25 μg of *PB-c-MYC*, (2) 0.25 μg of *PB-HRAS*^{G12V}, (3) 10 μg of either *PB-hFIXIA* or *PB-hFIXIA-miR-20a*, and (4) 2.25 μg of hyperactive PB-encoding plasmid. After 6 weeks of treatment, total extracted RNA from mouse liver tissues was used as a template for qRT-PCR using primers targeting 95 genes that are known to be associated with hepatocarcinogenesis. Total proteins were also extracted to compare the target protein expression level between *PB-hFIXIA* an *PB-hFIXIA-miR-20a*-transfected HCC groups. (A) Representative image and (B) quantitative Pten protein expression normalized to Gapdh (glyceraldehyde 3-phosphate dehydrogenase) expression from western blotting analysis. Graph presents the mean ± SEM of data obtained from individual mice; Mann-Whitney U test (n.s., not significant; *$p < 0.05$) (*PB-hFIXIA*, n = 6 mice; *PB-hFIXIA-miR-20a*, n = 6 mice). (C) ELISA analysis of Pten was performed to compare the protein expression level among all treatments. Graph presents the mean ± SEM of data obtained from individual mice; Mann-Whitney U test (n.s., not significant; **$p < 0.01$) (*PB-hFIXIA*, n = 6 mice; *PB-hFIXIA-miR-20a*, n = 6 mice). (D) Heatmap representing $\log_2$ fold change of all 95 gene expression profiles from *PB-hFIXIA*- and *PB-hFIXIA-miR-*

(legend continued on next page)

described by Beer et al.[81] Whereas both models result in rapid-onset HCC, the current *PB-c-MYC* and *PB-HRAS*^{G12V} HCC model did not require a transgenic model as in the case of the Tet-regulatable *c-MYC* transgenic mouse models used in the Beer et al. study. Hence, liver-specific somatic overexpression of oncogenes using the *PB* transposon platform provides a rapid, cost-effective, and relatively straightforward alternative to viral vector-mediated and transgenic HCC mouse models and obviates time-consuming and elaborate breeding schemes for different transgenic mouse strains. Moreover, these different HCC models likely contribute to rapid HCC development through different molecular pathways, which may provide new complementary insights into HCC development. A low level of shRNA expression causes gross perturbation of the *miR* signatures in the liver of the *c-MYC* transgenic mice, regardless of the shRNA type or specificity, whereas the current *HRAS*^{G12V}*/c-MYC* model results in different molecular signatures. The initial objective of the Beer et al. study was to selectively downregulate the expression of the tumor-suppressor gene p53 using p53-specific shRNA while conditionally expressing the transgenic *c-MYC* oncogene. As expected, the shRNAs silenced hepatic p53 and accelerated liver tumorigenesis when *c-MYC* was concurrently expressed. One of the unexpected and intriguing findings of the Beer et al. study was that various irrelevant control shRNAs (i.e., directed against hepatitis B virus surface antigen against or α1-antitrypsin) similarly induced a rapid onset of tumorigenesis, comparable to carbon tetrachloride (CCl_4), a potent carcinogen. Even marginal shRNA doses can already trigger histologically detectable hepatotoxicity and increased hepatocyte apoptosis. This suggests that the accelerated effect of shRNA on tumorigenesis is not shRNA-specific and may be due to a general cytotoxic effect that nonspecifically increased hepatocyte proliferation. In contrast, in our current study we demonstrated that the tumor suppressor effect of *miR-20a* is *miR-20a*-specific and has not been observed with any other *miR* that was tested, at least in the DEN HCC model. Hence, modulating tumorigenicity following *miR* overexpression may be dependent on specific *miR*s, whereas shRNA overexpression may influence tumorigenicity in a more general, non-specific fashion, perhaps by interfering with the cellular RNA interference (RNAi) machinery.[80] In addition, it offers a relatively short latency period compared to that of DEN-induced HCC, which usually requires 9–12 months.[36] Alternatively, other transposon systems, such as *Sleeping Beauty*, can be used to selectively express oncogenes in the liver.[50,84–88] However, a comparative analysis of different transposon systems revealed that hyPB led to an approximately 10-fold improvement in transgene expression compared to that with SB100X, thus suggesting a potential advantage of the hyPB transposon system for *in vivo* sustained gene expression.[89] This increased expression likely reflects an increase in transposon copy number per se rather than an increased mRNA expression level per transposon copy. Nevertheless, the SB system may yield a more random integration pattern, whereas PB transposons favor integration into genes.[90,91] Another advantage of the current system is that the synthetic hepatocyte-specific promoter allows for selective expression in only hepatocytes, avoiding undesirable effects or interfering tumor lesions in non-hepatocytes or ectopic tissue.[28–30,92]

The rapid-onset *HRAS*^{G12V}*/c-MYC* HCC model provides proof that the *HRAS*^{G12V} and *c-MYC* oncogenes cooperate in the development of HCC. This is consistent with previous studies showing that dysregulation of the Ras and c-Myc oncogene-dependent pathways promotes malignant transformation and tumor progression in the liver.[41,42] Our data suggests that the cooperative effects on cancer development mediated by the Ras/MAPK pathway and c-MYC may require c-MYC stabilization and Ras/MAPK/ERK signaling, which ultimately contributes to hepatocarcinogenesis.[93–95] This is supported by a substantial upregulation and multiple functional interactions of *Aurka* in mice overexpressing *HRAS*^{G12V} and *c-MYC* as observed in the current study. Phosphorylated c-MYC forms a protein complex with Aurka that stabilizes c-MYC.[96] Moreover, c-MYC induces *Aurka* mRNA expression and Aurka induces *c-MYC* mRNA expression, suggesting a positive feedback loop.[97] In addition, Aurka binds to HRas and further induces ERK phosphorylation through Ras/MAPK signaling.[98,99] *Akt1*, one of the highly interactive differentially expressed genes during *HRAS*^{G12V}*/c-MYC* HCC development, may prevent c-MYC degradation through Ras-driven activation of Akt.[100] Upregulation of *Cdc20* and *Igf2* following *HRAS*^{G12V} and *c-MYC* overexpression could perturb cell cycle regulation at the G_2/M phase and drive hepatocyte proliferation in mice, ultimately contributing to HCC.[101,102] In contrast, rapid-onset HCC development was found to not depend on the cooperation between *HRAS*^{G12V} and the *MDM2* or *MDM4* oncogenes.[43,44] This is in contrast to what has been observed in other tumors, such as colon carcinoma and melanomas. Indeed, in these cases, *RAS* is frequently activated with the concomitant overexpression of *MDM2* and/or *MDM4*, suggesting an important role of the *MDM2/MDM4* axis in inhibiting p53-dependent arrest in RAS-expressing cells.[103,104] Consistent with previous studies, overexpression of Ras and c-Myc further suppresses fatty acid metabolism by decreasing the expression of enzymes that are responsible for fatty acid accumulation and degradation.[50] In addition, c-Myc-mediated liver tumorigenesis is known to downregulate the expression of glutamine synthetase (Glul) and subsequently reduce glutamine synthesis.[105]

One of the merits of the slow- and rapid-onset HCC models described in the present study is that they obviate the need for orthotopic transplantation of transformed HCC cell lines, which does not mimic natural HCC initiation and progression.[106–108] Orthotopic transplantation typically involves subcutaneous implantation of already

20a-treated HCC groups. Genes that showed $p < 0.05$ for differential expression were defined as differentially expressed genes (DEGs); otherwise, genes were defined as non-differentially expressed genes (non-DEGs). Red and blue indicate upregulation and downregulation of the genes, respectively. DEGs were ranked based on fold difference (from high to low), and the number on the left of heatmap indicates an average fold difference (*PB-hFIXIA-miR-20a*, n = 4 mice; *PB-hFIXIA*, n = 4 mice). (E) Protein-protein interaction (PPI) networks of all DEGs of *PB-hFIXIA-miR-20a*-transfected HCC group versus *PB-hFIXIA* HCC group generated by the STRING database.

established HCC cell lines in a non-natural context and microenvironment and does not allow investigation of the early steps of HCC tumor initiation.[109] The models used in the current study overcome these limitations, and the results demonstrate unequivocally that *miR-20a* inhibits HCC initiation and progression in both the slow- and rapid-onset HCC models, which more closely mimic the natural context and microenvironment that foster HCC development. To our knowledge, no prior study has assessed the impact of overexpressing *miR*s using transposon systems on tumor initiation and progression in similar HCC mouse models that are based on *de novo* carcinogenesis. Moreover, the current study complements previous studies showing that *Sleeping Beauty* transposons can be used to express *miR*s in pulmonary fibrosis mouse models.[110]

The current study strengthens the diagnostic, prognostic, and therapeutic relevance of *miR-20a* in HCC. In particular, it supports the notion that *miR-20a* overexpression is associated with a more favorable prognosis in patients with HCC compared to that in patients who have only low or no *miR-20a* expression in their HCC biopsies. Moreover, the delivery of *miR-20a* may offer new therapeutic perspectives for the treatment of HCC. Recently, the first phase I clinical trial of *miR* therapy using liposome-based delivery was launched to evaluate the safety of treatment in patients with primary liver cancer (ClinicalTrials.gov: NCT01829971), and it may be applicable to *miR-20a*. Alternatively, the use of folic acid-modified nanoparticle-like lipid-based protocells was shown to be an effective method for the targeted delivery of transposons into cancer cells in a xenograft model, resulting in an *in vivo* transfection efficiency of up to 35%.[111] Ideally, the sustained and robust expression of *miR-20a* may be preferred to increase the therapeutic efficacy and prevent HCC recurrence. The presence of a gap junction allows the intracellular *miR* transfer between transfected cells and non-transfected adjacent cells, thereby potentially increasing its therapeutic impact.[112] Ultimately, this study may aid in the development of other clinically relevant gene delivery platforms, such as adeno-associated viral vectors or lentiviral vectors, to achieve sustained *miR-20a* expression in patients with HCC.[80,113,114]

MATERIALS AND METHODS

PB Transposon and Transposase Constructs

The PB transposon backbone used in this study was previously developed by our group.[30] To generate the PB transposons harboring *miR-17-92* cluster-derived *miR*s, specifically including *miR-17*, *miR-18a*, *miR-19a*, *miR-20a*, *miR-19b-1*, and *miR-92a-1*, the respective *miR*s flanked with approximately 50–200 bp of genomic sequences from mouse genomic DNA were first PCR amplified and subsequently cloned into the 1.4 kb-truncated human factor IX (*hFIX*) intron 1 (*intron IA*), namely *hFIXIA* (Table S3). The transgenes are flanked by truncated optimized IRs (IR_{micros}) (Figures 1B and 1C) composed of the 40 bp of 5′ and 67 bp of 3′ IRs.[115] The expression of the oncogenes was driven by the liver-specific chimeric promoter containing the TTR_{min} promoter as well as *HS-CRM8*.[28–30] The bovine growth hormone polyadenylation site (bGH-polyA) functioned as a terminating signal. The hyperactive PB transposase was used with the PB transposons for efficient transgene integration.[30] The coding sequences of four oncogenes, including *c-MYC*, $HRAS^{G12V}$, *MDM2*, and *MDM4*, were PCR amplified using specific primers harboring the NheI/BglII restriction sites and Phusion hot start high-fidelity DNA polymerase (Thermo Fisher Scientific, Merelbeke, Belgium) activity (Figure 1C) and cloned into the corresponding sites of the PB transposon plasmid.[30] For efficient *in vivo* transposition, we employed the hyperactive version of PB transposase containing 7 aa substitutions, which can improve transgene integration up to 8-fold compared to that with wild-type transposase.[116]

Animal Experiments

C57BL/6JRj male mice were purchased from Janvier (France) and Taconic (Denmark). All animal procedures were approved by the Institutional Animal Ethics Committee of the Free University of Brussels (VUB) (Brussels, Belgium) and the University of Leuven (Leuven, Belgium). Husbandry was carried out in individually ventilated Thoren cages that contained hygienic animal bedding from Lignocel. Temperature was maintained at approximately 21°C with 50%–60% humidity. Animals were fed SsniFF laboratory animal food (ABEDD Vertriebs, Vienna, Austria) *ad libitum*. For ectopic gene expression in mice, the PB transposons carrying transgenes were co-delivered with hyperactive-PB transposase-encoding plasmids (2:1 molar ratio of transposon/transposase) by hydrodynamic injection through the tail veins of 6-week-old mice. For DEN-induced hepatocarcinogenesis, 12.5 mg/kg body weight of DEN (Sigma-Aldrich, Diegem, Belgium) was injected intraperitoneally (i.p.) into 14-day-old mice.[117] Four weeks later, mice were hydrodynamically injected with the transposon plasmids if required, whole blood was collected into buffered citrate by phlebotomy of the retro-orbital plexus, and the citrated plasma was stored at −80°C. According to the experimental setting, the gross morphology and tumor formation were assessed after euthanasia to determine the hepatic tumor incidence by enumerating the total numbers of tumor nodules, macroscopically measuring total sizes of hepatic tumor nodules, and weighing the total mass of gross liver tissues. The data were collected for further analysis and statistics.

Statistical Analysis

GraphPad software (GraphPad, La Jolla, CA, USA) was used for data analysis. A two-tailed independent Student's t test was performed when the assumptions were valid, and the non-parametric Mann-Whitney U test was applied when the distribution of data was not normal and two variances were not equivalent. Differences in Kaplan-Meier survival curves from two populations were assessed to determine statistical significance by the log-rank test. Results are shown as the mean ± standard error of mean (SEM). n.s., not significant; *$p < 0.05$, **$p < 0.01$, ***$p < 0.001$, ****$p < 0.0001$.

SUPPLEMENTAL INFORMATION

Supplemental Information can be found online at https://doi.org/10.1016/j.omtn.2020.01.015.

AUTHOR CONTRIBUTIONS

J.T., M.D.M., and W.T. performed and designed the experiments, collected and processed the data, and wrote part of the paper.

E.S.-K. and J.K. performed the experiments and/or collected and processed the data. J.A.V.G. collected the data. T.V. and M.K.C. designed the experiments, analyzed the data, wrote and approved the paper, and led the study. T.V. and M.K.C. applied for and obtained financial support for this study.

CONFLICTS OF INTEREST

The authors declare no competing interests.

ACKNOWLEDGMENTS

This work was supported by the Fonds voor Wetenschappelijk Onderzoek (FWO), the VUB Strategic Research Program "Groeier", the VUB Industrieel Onderzoeksfonds (Groups of Expertise in Applied Research [GEAR], the VUB Geconcerteerde Onderzoek Acties (GOA) and the Stichting Tegen Kanker (STK) to M.K.C. and T.V.; M.D.M. and J.T. were supported by a FWO Aspirant Grant. We thank Ann Demarre for technical assistance.

REFERENCES

1. Bartel, D.P. (2004). MicroRNAs: genomics, biogenesis, mechanism, and function. Cell *116*, 281–297.
2. Calin, G.A., and Croce, C.M. (2006). MicroRNA signatures in human cancers. Nat. Rev. Cancer *6*, 857–866.
3. Calin, G.A., Dumitru, C.D., Shimizu, M., Bichi, R., Zupo, S., Noch, E., Aldler, H., Rattan, S., Keating, M., Rai, K., et al. (2002). Frequent deletions and down-regulation of micro-RNA genes *miR15* and *miR16* at 13q14 in chronic lymphocytic leukemia. Proc. Natl. Acad. Sci. USA *99*, 15524–15529.
4. Black, J.C., Zhang, H., Kim, J., Getz, G., and Whetstine, J.R. (2016). Regulation of transient site-specific copy gain by microRNA. J. Biol. Chem. *291*, 4862–4871.
5. Czubak, K., Lewandowska, M.A., Klonowska, K., Roszkowski, K., Kowalewski, J., Figlerowicz, M., and Kozlowski, P. (2015). High copy number variation of cancer-related microRNA genes and frequent amplification of DICER1 and DROSHA in lung cancer. Oncotarget *6*, 23399–23416.
6. Xia, E., Kanematsu, S., Suenaga, Y., Elzawahry, A., Kondo, H., Otsuka, N., Moriya, Y., Iizasa, T., Kato, M., Yoshino, I., and Yokoi, S. (2018). MicroRNA induction by copy number gain is associated with poor outcome in squamous cell carcinoma of the lung. Sci. Rep. *8*, 15363.
7. Hayes, J., Peruzzi, P.P., and Lawler, S. (2014). MicroRNAs in cancer: biomarkers, functions and therapy. Trends Mol. Med. *20*, 460–469.
8. Hamam, R., Hamam, D., Alsaleh, K.A., Kassem, M., Zaher, W., Alfayez, M., Aldahmash, A., and Alajez, N.M. (2017). Circulating microRNAs in breast cancer: novel diagnostic and prognostic biomarkers. Cell Death Dis. *8*, e3045.
9. Long, Q., Johnson, B.A., Osunkoya, A.O., Lai, Y.H., Zhou, W., Abramovitz, M., Xia, M., Bouzyk, M.B., Nam, R.K., Sugar, L., et al. (2011). Protein-coding and microRNA biomarkers of recurrence of prostate cancer following radical prostatectomy. Am. J. Pathol. *179*, 46–54.
10. Calin, G.A., Sevignani, C., Dumitru, C.D., Hyslop, T., Noch, E., Yendamuri, S., Shimizu, M., Rattan, S., Bullrich, F., Negrini, M., and Croce, C.M. (2004). Human microRNA genes are frequently located at fragile sites and genomic regions involved in cancers. Proc. Natl. Acad. Sci. USA *101*, 2999–3004.
11. McGlynn, K.A., and London, W.T. (2011). The global epidemiology of hepatocellular carcinoma: present and future. Clin. Liver Dis. *15*, 223–243, vii–x.
12. Gomaa, A.I., Khan, S.A., Toledano, M.B., Waked, I., and Taylor-Robinson, S.D. (2008). Hepatocellular carcinoma: epidemiology, risk factors and pathogenesis. World J. Gastroenterol. *14*, 4300–4308.
13. Zhu, H., Han, C., and Wu, T. (2015). miR-17-92 cluster promotes hepatocarcinogenesis. Carcinogenesis *36*, 1213–1222.
14. Fan, M.Q., Huang, C.B., Gu, Y., Xiao, Y., Sheng, J.X., and Zhong, L. (2013). Decrease expression of microRNA-20a promotes cancer cell proliferation and predicts poor survival of hepatocellular carcinoma. J. Exp. Clin. Cancer Res. *32*, 21.
15. Chen, G.S., Zhou, N., Li, J.Q., Li, T., Zhang, Z.Q., and Si, Z.Z. (2016). Restoration of miR-20a expression suppresses cell proliferation, migration, and invasion in HepG2 cells. OncoTargets Ther. *9*, 3067–3076.
16. Xu, W.P., Yi, M., Li, Q.Q., Zhou, W.P., Cong, W.M., Yang, Y., Ning, B.F., Yin, C., Huang, Z.W., Wang, J., et al. (2013). Perturbation of microRNA-370/Lin-28 homolog A/nuclear factor kappa B regulatory circuit contributes to the development of hepatocellular carcinoma. Hepatology *58*, 1977–1991.
17. Moshiri, F., Callegari, E., D'Abundo, L., Corrà, F., Lupini, L., Sabbioni, S., and Negrini, M. (2014). Inhibiting the oncogenic mir-221 by microRNA sponge: toward microRNA-based therapeutics for hepatocellular carcinoma. Gastroenterol. Hepatol. Bed Bench *7*, 43–54.
18. Yang, Y.F., Wang, F., Xiao, J.J., Song, Y., Zhao, Y.Y., Cao, Y., Bei, Y.H., and Yang, C.Q. (2014). miR-222 overexpression promotes proliferation of human hepatocellular carcinoma HepG2 cells by downregulating p27. Int. J. Clin. Exp. Med. *7*, 893–902.
19. Li, Y., Tan, W., Neo, T.W., Aung, M.O., Wasser, S., Lim, S.G., and Tan, T.M. (2009). Role of the *miR-106b-25* microRNA cluster in hepatocellular carcinoma. Cancer Sci. *100*, 1234–1242.
20. Yen, C.S., Su, Z.R., Lee, Y.P., Liu, I.T., and Yen, C.J. (2016). miR-106b promotes cancer progression in hepatitis B virus-associated hepatocellular carcinoma. World J. Gastroenterol. *22*, 5183–5192.
21. Ohta, K., Hoshino, H., Wang, J., Ono, S., Iida, Y., Hata, K., Huang, S.K., Colquhoun, S., and Hoon, D.S. (2015). MicroRNA-93 activates c-Met/PI3K/Akt pathway activity in hepatocellular carcinoma by directly inhibiting PTEN and CDKN1A. Oncotarget *6*, 3211–3224.
22. Wang, C., Wang, X., Su, Z., Fei, H., Liu, X., and Pan, Q. (2015). miR-25 promotes hepatocellular carcinoma cell growth, migration and invasion by inhibiting RhoGDI1. Oncotarget *6*, 36231–36244.
23. Cui, W., Huang, Z., He, H., Gu, N., Qin, G., Lv, J., Zheng, T., Sugimoto, K., and Wu, Q. (2015). miR-1188 at the imprinted *Dlk1-Dio3* domain acts as a tumor suppressor in hepatoma cells. Mol. Biol. Cell *26*, 1416–1427.
24. Thurnherr, T., Mah, W.C., Lei, Z., Jin, Y., Rozen, S.G., and Lee, C.G. (2016). Differentially expressed miRNAs in hepatocellular carcinoma target genes in the genetic information processing and metabolism pathways. Sci. Rep. *6*, 20065.
25. Gramantieri, L., Fornari, F., Callegari, E., Sabbioni, S., Lanza, G., Croce, C.M., Bolondi, L., and Negrini, M. (2008). MicroRNA involvement in hepatocellular carcinoma. J. Cell. Mol. Med. *12* (6A), 2189–2204.
26. Girard, M., Jacquemin, E., Munnich, A., Lyonnet, S., and Henrion-Caude, A. (2008). miR-122, a paradigm for the role of microRNAs in the liver. J. Hepatol. *48*, 648–656.
27. Murakami, Y., Yasuda, T., Saigo, K., Urashima, T., Toyoda, H., Okanoue, T., and Shimotohno, K. (2006). Comprehensive analysis of microRNA expression patterns in hepatocellular carcinoma and non-tumorous tissues. Oncogene *25*, 2537–2545.
28. Chuah, M.K., Petrus, I., De Bleser, P., Le Guiner, C., Gernoux, G., Adjali, O., Nair, N., Willems, J., Evens, H., Rincon, M.Y., et al. (2014). Liver-specific transcriptional modules identified by genome-wide in silico analysis enable efficient gene therapy in mice and non-human primates. Mol. Ther. *22*, 1605–1613.
29. Nair, N., Rincon, M.Y., Evens, H., Sarcar, S., Dastidar, S., Samara-Kuko, E., Ghandeharian, O., Man Viecelli, H., Thöny, B., De Bleser, P., et al. (2014). Computationally designed liver-specific transcriptional modules and hyperactive factor IX improve hepatic gene therapy. Blood *123*, 3195–3199.
30. Di Matteo, M., Samara-Kuko, E., Ward, N.J., Waddington, S.N., McVey, J.H., Chuah, M.K., and VandenDriessche, T. (2014). Hyperactive piggyBac transposons for sustained and robust liver-targeted gene therapy. Mol. Ther. *22*, 1614–1624.
31. Tipanee, J., VandenDriessche, T., and Chuah, M.K. (2017). Transposons: moving forward from preclinical studies to clinical trials. Hum. Gene Ther. *28*, 1087–1104.
32. Tipanee, J., Chai, Y.C., VandenDriessche, T., and Chuah, M.K. (2017). Preclinical and clinical advances in transposon-based gene therapy. Biosci. Rep. *37*, BSR20160614.

33. Cary, L.C., Goebel, M., Corsaro, B.G., Wang, H.G., Rosen, E., and Fraser, M.J. (1989). Transposon mutagenesis of baculoviruses: analysis of Trichoplusia ni transposon IFP2 insertions within the FP-locus of nuclear polyhedrosis viruses. Virology *172*, 156–169.

34. VandenDriessche, T., Ivics, Z., Izsvák, Z., and Chuah, M.K. (2009). Emerging potential of transposons for gene therapy and generation of induced pluripotent stem cells. Blood *114*, 1461–1468.

35. Di Matteo, M., Mátrai, J., Belay, E., Firdissa, T., Vandendriessche, T., and Chuah, M.K. (2012). PiggyBac toolbox. Methods Mol. Biol. *859*, 241–254.

36. Heindryckx, F., Colle, I., and Van Vlierberghe, H. (2009). Experimental mouse models for hepatocellular carcinoma research. Int. J. Exp. Pathol. *90*, 367–386.

37. Seyhan, A.A. (2016). A multiplexed miRNA and transgene expression platform for simultaneous repression and expression of protein coding sequences. Mol. Biosyst. *12*, 295–312.

38. Haley, B., Foys, B., and Levine, M. (2010). Vectors and parameters that enhance the efficacy of RNAi-mediated gene disruption in transgenic *Drosophila*. Proc. Natl. Acad. Sci. USA *107*, 11435–11440.

39. White, M.D., Milne, R.V., and Nolan, M.F. (2011). A molecular toolbox for rapid generation of viral vectors to up- or down-regulate neuronal gene expression in vivo. Front. Mol. Neurosci. *4*, 8.

40. Askou, A.L., Aagaard, L., Kostic, C., Arsenijevic, Y., Hollensen, A.K., Bek, T., Jensen, T.G., Mikkelsen, J.G., and Corydon, T.J. (2015). Multigenic lentiviral vectors for combined and tissue-specific expression of miRNA- and protein-based antiangiogenic factors. Mol. Ther. Methods Clin. Dev. *2*, 14064.

41. Parsons, B.L., Culp, S.J., Manjanatha, M.G., and Heflich, R.H. (2002). Occurrence of H-ras codon 61 CAA to AAA mutation during mouse liver tumor progression. Carcinogenesis *23*, 943–948.

42. Murakami, H., Sanderson, N.D., Nagy, P., Marino, P.A., Merlino, G., and Thorgeirsson, S.S. (1993). Transgenic mouse model for synergistic effects of nuclear oncogenes and growth factors in tumorigenesis: interaction of *c-myc* and transforming growth factor α in hepatic oncogenesis. Cancer Res. *53*, 1719–1723.

43. Pellegrino, R., Calvisi, D.F., Neumann, O., Kolluru, V., Wesely, J., Chen, X., Wang, C., Wuestefeld, T., Ladu, S., Elgohary, N., et al. (2014). EEF1A2 inactivates p53 by way of PI3K/AKT/mTOR-dependent stabilization of MDM4 in hepatocellular carcinoma. Hepatology *59*, 1886–1899.

44. Meng, X., Franklin, D.A., Dong, J., and Zhang, Y. (2014). MDM2-p53 pathway in hepatocellular carcinoma. Cancer Res. *74*, 7161–7167.

45. Olofson, A.M., Gonzalo, D.H., Chang, M., and Liu, X. (2018). Steatohepatitic variant of hepatocellular carcinoma: a focused review. Gastroenterol. Res. *11*, 391–396.

46. Yeh, M.M., Liu, Y., and Torbenson, M. (2015). Steatohepatitic variant of hepatocellular carcinoma in the absence of metabolic syndrome or background steatosis: a clinical, pathological, and genetic study. Hum. Pathol. *46*, 1769–1775.

47. Jeong, H., Mason, S.P., Barabási, A.L., and Oltvai, Z.N. (2001). Lethality and centrality in protein networks. Nature *411*, 41–42.

48. Said, M.R., Begley, T.J., Oppenheim, A.V., Lauffenburger, D.A., and Samson, L.D. (2004). Global network analysis of phenotypic effects: protein networks and toxicity modulation in *Saccharomyces cerevisiae*. Proc. Natl. Acad. Sci. USA *101*, 18006–18011.

49. Ideker, T., and Sharan, R. (2008). Protein networks in disease. Genome Res. *18*, 644–652.

50. Xin, B., Yamamoto, M., Fujii, K., Ooshio, T., Chen, X., Okada, Y., Watanabe, K., Miyokawa, N., Furukawa, H., and Nishikawa, Y. (2017). Critical role of Myc activation in mouse hepatocarcinogenesis induced by the activation of AKT and RAS pathways. Oncogene *36*, 5087–5097.

51. Luo, Y., Ren, F., Liu, Y., Shi, Z., Tan, Z., Xiong, H., Dang, Y., and Chen, G. (2015). Clinicopathological and prognostic significance of high Ki-67 labeling index in hepatocellular carcinoma patients: a meta-analysis. Int. J. Clin. Exp. Med. *8*, 10235–10247.

52. Majumder, S., Roy, S., Kaffenberger, T., Wang, B., Costinean, S., Frankel, W., Bratasz, A., Kuppusamy, P., Hai, T., Ghoshal, K., and Jacob, S.T. (2010). Loss of metallothionein predisposes mice to diethylnitrosamine-induced hepatocarcinogenesis by activating NF-κB target genes. Cancer Res. *70*, 10265–10276.

53. Agarwal, V., Bell, G.W., Nam, J.W., and Bartel, D.P. (2015). Predicting effective microRNA target sites in mammalian mRNAs. eLife *4*, 4.

54. Loeb, G.B., Khan, A.A., Canner, D., Hiatt, J.B., Shendure, J., Darnell, R.B., Leslie, C.S., and Rudensky, A.Y. (2012). Transcriptome-wide miR-155 binding map reveals widespread noncanonical microRNA targeting. Mol. Cell *48*, 760–770.

55. Schug, J., McKenna, L.B., Walton, G., Hand, N., Mukherjee, S., Essuman, K., Shi, Z., Gao, Y., Markley, K., Nakagawa, M., et al. (2013). Dynamic recruitment of microRNAs to their mRNA targets in the regenerating liver. BMC Genomics *14*, 264.

56. Zhang, X., Zuo, X., Yang, B., Li, Z., Xue, Y., Zhou, Y., Huang, J., Zhao, X., Zhou, J., Yan, Y., et al. (2014). MicroRNA directly enhances mitochondrial translation during muscle differentiation. Cell *158*, 607–619.

57. Michelotti, G.A., Machado, M.V., and Diehl, A.M. (2013). NAFLD, NASH and liver cancer. Nat. Rev. Gastroenterol. Hepatol. *10*, 656–665.

58. Shearn, C.T., and Petersen, D.R. (2015). Understanding the tumor suppressor PTEN in chronic alcoholism and hepatocellular carcinoma. Adv. Exp. Med. Biol. *815*, 173–184.

59. Ryan, K.M., Ernst, M.K., Rice, N.R., and Vousden, K.H. (2000). Role of NF-κB in p53-mediated programmed cell death. Nature *404*, 892–897.

60. Micheau, O., and Tschopp, J. (2003). Induction of TNF receptor I-mediated apoptosis via two sequential signaling complexes. Cell *114*, 181–190.

61. Connor, F., Rayner, T.F., Aitken, S.J., Feig, C., Lukk, M., Santoyo-Lopez, J., and Odom, D.T. (2018). Mutational landscape of a chemically-induced mouse model of liver cancer. J. Hepatol. *69*, 840–850.

62. Wang, Y., Zhao, Y.R., Zhang, A.Y., Ma, J., Wang, Z.Z., and Zhang, X. (2017). Targeting of miR-20a against CFLAR to potentiate TRAIL-induced apoptotic sensitivity in HepG2 cells. Eur. Rev. Med. Pharmacol. Sci. *21*, 2980.

63. Cheng, E.H., Wei, M.C., Weiler, S., Flavell, R.A., Mak, T.W., Lindsten, T., and Korsmeyer, S.J. (2001). BCL-2, BCL-X_L sequester BH3 domain-only molecules preventing BAX- and BAK-mediated mitochondrial apoptosis. Mol. Cell *8*, 705–711.

64. Watanabe, J., Kushihata, F., Honda, K., Mominoki, K., Matsuda, S., and Kobayashi, N. (2002). Bcl-xL overexpression in human hepatocellular carcinoma. Int. J. Oncol. *21*, 515–519.

65. Trisciuoglio, D., Tupone, M.G., Desideri, M., Di Martile, M., Gabellini, C., Buglioni, S., Pallocca, M., Alessandrini, G., D'Aguanno, S., and Del Bufalo, D. (2017). BCL-X_L overexpression promotes tumor progression-associated properties. Cell Death Dis. *8*, 3216.

66. Yan, Q., Zhang, Z.F., Chen, X.P., Gutmann, D.H., Xiong, M., Xiao, Z.Y., and Huang, Z.Y. (2008). Reduced T-cadherin expression and promoter methylation are associated with the development and progression of hepatocellular carcinoma. Int. J. Oncol. *32*, 1057–1063.

67. Baek, J.Y., Morris, S.M., Campbell, J., Fausto, N., Yeh, M.M., and Grady, W.M. (2010). TGF-β inactivation and TGF-α overexpression cooperate in an in vivo mouse model to induce hepatocellular carcinoma that recapitulates molecular features of human liver cancer. Int. J. Cancer *127*, 1060–1071.

68. Khetani, S.R., Chen, A.A., Ranscht, B., and Bhatia, S.N. (2008). T-cadherin modulates hepatocyte functions in vitro. FASEB J. *22*, 3768–3775.

69. Lin, J., Chen, Z., Huang, Z., Chen, F., Ye, Z., Lin, S., and Wang, W. (2017). Upregulation of T-cadherin suppresses cell proliferation, migration and invasion of gastric cancer *in vitro*. Exp. Ther. Med. *14*, 4194–4200.

70. Singh, B., and Coffey, R.J. (2014). From wavy hair to naked proteins: the role of transforming growth factor alpha in health and disease. Semin. Cell Dev. Biol. *28*, 12–21.

71. Hennig, M., Yip-Schneider, M.T., Klein, P., Wentz, S., Matos, J.M., Doyle, C., Choi, J., Wu, H., O'Mara, A., Menze, A., et al. (2009). Ethanol-TGFα-MEK signaling promotes growth of human hepatocellular carcinoma. J. Surg. Res. *154*, 187–195.

72. Schausberger, E., Hufnagl, K., Parzefall, W., Gerner, C., Kandioler-Eckersberger, D., Wrba, F., Klimpfinger, M., Schulte-Hermann, R., and Grasl-Kraupp, B. (2004). Inherent growth advantage of (pre)malignant hepatocytes associated with nuclear translocation of pro-transforming growth factor α. Br. J. Cancer *91*, 1955–1963.

73. Schaff, Z., Hsia, C.C., Sarosi, I., and Tabor, E. (1994). Overexpression of transforming growth factor-alpha in hepatocellular carcinoma and focal nodular hyperplasia from European patients. Hum. Pathol. *25*, 644–651.

74. Chung, Y.H., Kim, J.A., Song, B.C., Lee, G.C., Koh, M.S., Lee, Y.S., Lee, S.G., and Suh, D.J. (2000). Expression of transforming growth factor-alpha mRNA in livers of patients with chronic viral hepatitis and hepatocellular carcinoma. Cancer *89*, 977–982.

75. Wang, K. (2014). Molecular mechanisms of hepatic apoptosis. Cell Death Dis. *5*, e996.

76. Guicciardi, M.E., and Gores, G.J. (2005). Apoptosis: a mechanism of acute and chronic liver injury. Gut *54*, 1024–1033.

77. Xue, W., Chen, S., Yin, H., Tammela, T., Papagiannakopoulos, T., Joshi, N.S., Cai, W., Yang, G., Bronson, R., Crowley, D.G., et al. (2014). CRISPR-mediated direct mutation of cancer genes in the mouse liver. Nature *514*, 380–384.

78. Horie, Y., Suzuki, A., Kataoka, E., Sasaki, T., Hamada, K., Sasaki, J., Mizuno, K., Hasegawa, G., Kishimoto, H., Iizuka, M., et al. (2004). Hepatocyte-specific Pten deficiency results in steatohepatitis and hepatocellular carcinomas. J. Clin. Invest. *113*, 1774–1783.

79. Xu, Z., Hu, J., Cao, H., Pilo, M.G., Cigliano, A., Shao, Z., Xu, M., Ribback, S., Dombrowski, F., Calvisi, D.F., and Chen, X. (2018). Loss of Pten synergizes with c-Met to promote hepatocellular carcinoma development via mTORC2 pathway. Exp. Mol. Med. *50*, e417.

80. Grimm, D., Streetz, K.L., Jopling, C.L., Storm, T.A., Pandey, K., Davis, C.R., Marion, P., Salazar, F., and Kay, M.A. (2006). Fatality in mice due to oversaturation of cellular microRNA/short hairpin RNA pathways. Nature *441*, 537–541.

81. Beer, S., Bellovin, D.I., Lee, J.S., Komatsubara, K., Wang, L.S., Koh, H., Börner, K., Storm, T.A., Davis, C.R., Kay, M.A., et al. (2010). Low-level shRNA cytotoxicity can contribute to MYC-induced hepatocellular carcinoma in adult mice. Mol. Ther. *18*, 161–170.

82. Marquez, J., Fernandez-Pineiro, I., Arauzo-Bravo, M.J., Poschmann, G., Stuhler, K., Khatib, A.M., Sanchez, A., Unda, F., Ibarretxe, G., Bernales, I., et al. (2018). Targeting liver sinusoidal endothelial cells with miR-20a-loaded nanoparticles reduces murine colon cancer metastasis to the liver. Int. J. Cancer *143*, 709–719.

83. Pineau, P., Volinia, S., McJunkin, K., Marchio, A., Battiston, C., Terris, B., Mazzaferro, V., Lowe, S.W., Croce, C.M., and Dejean, A. (2010). miR-221 overexpression contributes to liver tumorigenesis. Proc. Natl. Acad. Sci. USA *107*, 264–269.

84. Ivics, Z., Hackett, P.B., Plasterk, R.H., and Izsvák, Z. (1997). Molecular reconstruction of *Sleeping Beauty*, a *Tc1*-like transposon from fish, and its transposition in human cells. Cell *91*, 501–510.

85. Mátés, L., Chuah, M.K., Belay, E., Jerchow, B., Manoj, N., Acosta-Sanchez, A., Grzela, D.P., Schmitt, A., Becker, K., Matrai, J., et al. (2009). Molecular evolution of a novel hyperactive *Sleeping Beauty* transposase enables robust stable gene transfer in vertebrates. Nat. Genet. *41*, 753–761.

86. Yant, S.R., Meuse, L., Chiu, W., Ivics, Z., Izsvak, Z., and Kay, M.A. (2000). Somatic integration and long-term transgene expression in normal and haemophilic mice using a DNA transposon system. Nat. Genet. *25*, 35–41.

87. Carlson, C.M., Frandsen, J.L., Kirchhof, N., McIvor, R.S., and Largaespada, D.A. (2005). Somatic integration of an oncogene-harboring *Sleeping Beauty* transposon models liver tumor development in the mouse. Proc. Natl. Acad. Sci. USA *102*, 17059–17064.

88. Ju, H.L., Ahn, S.H., Kim, D.Y., Baek, S., Chung, S.I., Seong, J., Han, K.H., and Ro, S.W. (2013). Investigation of oncogenic cooperation in simple liver-specific transgenic mouse models using noninvasive in vivo imaging. PLoS ONE *8*, e59869.

89. Doherty, J.E., Huye, L.E., Yusa, K., Zhou, L., Craig, N.L., and Wilson, M.H. (2012). Hyperactive *piggyBac* gene transfer in human cells and in vivo. Hum. Gene Ther. *23*, 311–320.

90. Turchiano, G., Latella, M.C., Gogol-Döring, A., Cattoglio, C., Mavilio, F., Izsvák, Z., Ivics, Z., and Recchia, A. (2014). Genomic analysis of *Sleeping Beauty* transposon integration in human somatic cells. PLoS ONE *9*, e112712.

91. Huang, X., Guo, H.F., Tammana, S., Jung, Y.C., Mellgren, E., Bassi, P., et al. (2010). Corrigendum to "Gene transfer efficiency and genome-wide integration profiling of *Sleeping Beauty*, *Tol2*, and *piggyBac* transposons in human primary T cells". Mol. Ther. *18*, 2038.

92. Singh, K., Evens, H., Nair, N., Rincón, M.Y., Sarcar, S., Samara-Kuko, E., Chuah, M.K., and VandenDriessche, T. (2018). Efficient in vivo liver-directed gene editing using CRISPR/Cas9. Mol. Ther. *26*, 1241–1254.

93. Ho, C., Wang, C., Mattu, S., Destefanis, G., Ladu, S., Delogu, S., et al. (2012). AKT (v-akt murine thymoma viral oncogene homolog 1) and N-Ras (neuroblastoma ras viral oncogene homolog) coactivation in the mouse liver promotes rapid carcinogenesis by way of mTOR (mammalian target of rapamycin complex 1), FOXM1 (forkhead box M1)/SKP2, and c-Myc pathways. Hepatology *55*, 833–845.

94. Tsai, W.B., Aiba, I., Long, Y., Lin, H.K., Feun, L., Savaraj, N., and Kuo, M.T. (2012). Activation of Ras/PI3K/ERK pathway induces c-Myc stabilization to upregulate argininosuccinate synthetase, leading to arginine deiminase resistance in melanoma cells. Cancer Res. *72*, 2622–2633.

95. Yang, S., and Liu, G. (2017). Targeting the Ras/Raf/MEK/ERK pathway in hepatocellular carcinoma. Oncol. Lett. *13*, 1041–1047.

96. Dauch, D., Rudalska, R., Cossa, G., Nault, J.C., Kang, T.W., Wuestefeld, T., Hohmeyer, A., Imbeaud, S., Yevsa, T., Hoenicke, L., et al. (2016). A MYC-aurora kinase A protein complex represents an actionable drug target in p53-altered liver cancer. Nat. Med. *22*, 744–753.

97. Lu, L., Han, H., Tian, Y., Li, W., Zhang, J., Feng, M., and Li, Y. (2015). Aurora kinase A mediates c-Myc's oncogenic effects in hepatocellular carcinoma. Mol. Carcinog. *54*, 1467–1479.

98. Umstead, M., Xiong, J., Qi, Q., Du, Y., and Fu, H. (2017). Aurora kinase A interacts with H-Ras and potentiates Ras-MAPK signaling. Oncotarget *8*, 28359–28372.

99. Jacobsen, A., Bosch, L.J.W., Martens-de Kemp, S.R., Carvalho, B., Sillars-Hardebol, A.H., Dobson, R.J., de Rinaldis, E., Meijer, G.A., Abeln, S., Heringa, J., et al. (2018). Aurora kinase A (AURKA) interaction with Wnt and Ras-MAPK signalling pathways in colorectal cancer. Sci. Rep. *8*, 7522.

100. Bachireddy, P., Bendapudi, P.K., and Felsher, D.W. (2005). Getting at MYC through RAS. Clin. Cancer Res. *11*, 4278–4281.

101. Wang, M.J., Chen, F., Liu, Q.G., Liu, C.C., Yao, H., Yu, B., Zhang, H.B., Yan, H.X., Ye, Y., Chen, T., et al. (2018). Insulin-like growth factor 2 is a key mitogen driving liver repopulation in mice. Cell Death Dis. *9*, 26.

102. Li, J., Gao, J.Z., Du, J.L., Huang, Z.X., and Wei, L.X. (2014). Increased CDC20 expression is associated with development and progression of hepatocellular carcinoma. Int. J. Oncol. *45*, 1547–1555.

103. Gilkes, D.M., Pan, Y., Coppola, D., Yeatman, T., Reuther, G.W., and Chen, J. (2008). Regulation of MDMX expression by mitogenic signaling. Mol. Cell. Biol. *28*, 1999–2010.

104. Ries, S., Biederer, C., Woods, D., Shifman, O., Shirasawa, S., Sasazuki, T., McMahon, M., Oren, M., and McCormick, F. (2000). Opposing effects of Ras on p53: transcriptional activation of *mdm2* and induction of $p19^{ARF}$. Cell *103*, 321–330.

105. Yuneva, M.O., Fan, T.W.M., Allen, T.D., Higashi, R.M., Ferraris, D.V., Tsukamoto, T., Matés, J.M., Alonso, F.J., Wang, C., Seo, Y., et al. (2012). The metabolic profile of tumors depends on both the responsible genetic lesion and tissue type. Cell Metab. *15*, 157–170.

106. Werbeck, J.L., Thudi, N.K., Martin, C.K., Premanandan, C., Yu, L., Ostrowksi, M.C., and Rosol, T.J. (2014). Tumor microenvironment regulates metastasis and metastasis genes of mouse MMTV-PymT mammary cancer cells in vivo. Vet. Pathol. *51*, 868–881.

107. Zhao, X., Li, L., Starr, T.K., and Subramanian, S. (2017). Tumor location impacts immune response in mouse models of colon cancer. Oncotarget *8*, 54775–54787.

108. Burrell, J.S., Walker-Samuel, S., Boult, J.K., Baker, L.C., Jamin, Y., Halliday, J., Waterton, J.C., and Robinson, S.P. (2016). Investigating the vascular phenotype of subcutaneously and orthotopically propagated PC3 prostate cancer xenografts using combined carbogen ultrasmall superparamagnetic iron oxide MRI. Top. Magn. Reson. Imaging *25*, 237–243.

109. Chen, C.L., Wu, J.C., Chen, G.Y., Yuan, P.H., Tseng, Y.W., Li, K.C., Hwang, S.M., and Hu, Y.C. (2015). Baculovirus-mediated miRNA regulation to suppress hepatocellular carcinoma tumorigenicity and metastasis. Mol. Ther. *23*, 79–88.

110. Xiao, J., Meng, X.M., Huang, X.R., Chung, A.C., Feng, Y.L., Hui, D.S., Yu, C.M., Sung, J.J., and Lan, H.Y. (2012). miR-29 inhibits bleomycin-induced pulmonary fibrosis in mice. Mol. Ther. *20*, 1251–1260.

111. Ma, K., Fu, D., Yu, D., Cui, C., Wang, L., Guo, Z., and Mao, C. (2017). Targeted delivery of in situ PCR-amplified Sleeping Beauty transposon genes to cancer cells with lipid-based nanoparticle-like protocells. Biomaterials *121*, 55–63.

112. Zong, L., Zhu, Y., Liang, R., and Zhao, H.B. (2016). Gap junction mediated miRNA intercellular transfer and gene regulation: A novel mechanism for intercellular genetic communication. Sci. Rep. *6*, 19884.

113. Xie, J., Ameres, S.L., Friedline, R., Hung, J.H., Zhang, Y., Xie, Q., Zhong, L., Su, Q., He, R., Li, M., et al. (2012). Long-term, efficient inhibition of microRNA function in mice using rAAV vectors. Nat. Methods *9*, 403–409.

114. Brown, B.D., and Naldini, L. (2009). Exploiting and antagonizing microRNA regulation for therapeutic and experimental applications. Nat. Rev. Genet. *10*, 578–585.

115. Meir, Y.J., Weirauch, M.T., Yang, H.S., Chung, P.C., Yu, R.K., and Wu, S.C. (2011). Genome-wide target profiling of *piggyBac* and *Tol2* in HEK 293: pros and cons for gene discovery and gene therapy. BMC Biotechnol. *11*, 28.

116. Yusa, K., Zhou, L., Li, M.A., Bradley, A., and Craig, N.L. (2011). A hyperactive *piggyBac* transposase for mammalian applications. Proc. Natl. Acad. Sci. USA *108*, 1531–1536.

117. Vesselinovitch, S.D., and Mihailovich, N. (1983). Kinetics of diethylnitrosamine hepatocarcinogenesis in the infant mouse. Cancer Res. *43*, 4253–4259.